| | |
|---|---|
| Title | Design of novel visible light active photocatalyst materials: Surface modified TiO2 |
| Authors | Nolan, Michael;Iwaszuk, Anna;Lucid, Aoife K.;Carey, John J.;Fronzi, Marco |
| Publication date | 2016-02-02 |
| Original Citation | Nolan, M., Iwaszuk, A., Lucid, A. K., Carey, J. J. and Fronzi, M. (2016) 'Design of Novel Visible Light Active Photocatalyst Materials: Surface Modified TiO2', Advanced Materials, 28(27), pp. 5425-5446. doi: 10.1002/adma.201504894 |
| Type of publication | Article (peer-reviewed) |
| Link to publisher's version | 10.1002/adma.201504894 |
| Rights | © 2016 WILEY-VCH Verlag GmbH & Co. KGaA, Weinheim. This is the peer reviewed version of the following article: Nolan, M. et al. (2016) 'Design of Novel Visible Light Active Photocatalyst Materials: Surface Modified TiO2', Advanced Materials, 28(27), which has been published in final form at http://dx.doi.org/10.1002/adma.201504894. This article may be used for non-commercial purposes in accordance with Wiley Terms and Conditions for Self-Archiving. |
| Download date | 2024-05-04 08:22:04 |
| Item downloaded from | https://hdl.handle.net/10468/4939 |

DOI: 10.1002/ ((please add manuscript number))
Article type: Progress Report

# Design of novel visible light active photocatalyst materials: Surface modified $TiO_2$

*Michael Nolan*, Anna Iwaszuk, Aoife K. Lucid, John J. Carey and Marco Fronzi*

Dr. Michael Nolan, Dr. Anna Iwaszuk, Aoife K. Lucid, Dr. John J. Carey, Dr. Marco Fronzi
Tyndall National Institute, Lee Maltings, University College Cork, Cork, Ireland
michael.nolan@tyndall.ie

Keywords: Photocatalysis; $TiO_2$; density functional theory; surface modification; nanoclusters; red shift; photoexcitation; adsorption; oxidation; holes; electrons; SnO; PbO; NiO; CuO; $Fe_2O_3$; UV-vis; XPS; valence band

## Abstract

This progress review describes our work on the design of new $TiO_2$ based photocatalysts. The key concept is the formation of composite structures through the modification of anatase and rutile $TiO_2$ with molecular-sized nanoclusters of metals oxides. Our density functional theory (DFT) level simulations have been compared with experimental work synthesizing and characterizing surface modified $TiO_2$. We use DFT to show that nanoclusters of metal oxides such as $TiO_2$, $SnO/SnO_2$, $PbO/PbO_2$, ZnO and CuO are stable when adsorbed at rutile and anatase surfaces and can lead to a significant red shift in the absorption edge which will induce visible light absorption; this is the first requirement for a useful photocatalyst. We determine the origin of the red shift and the fate of excited electrons and holes. For p-block metal oxides the oxidation state of Sn and Pb can be used to modify the magnitude of the red shift and its mechanism. We describe comparisons of recent experimental studies of surface modified $TiO_2$ that validate our DFT simulations. These nanocluster-modified $TiO_2$ structures

form the basis of a new class of photocatalysts which will be useful in oxidation reactions and with a correct choice of nanocluster modified can be applied to other reactions.

## 1. Introduction

### 1.1 The grand challenges of the energy supply and $CO_2$ emissions.

Progress for mankind depends on securing and using energy sources, from wood to coal to oil/natural gas. However, these resources are non-renewable and combustion of fossil fuels emits $CO_2$. Fossil fuels are, however, an almost ideal fuel source, with high energy density and their ease of storage and distribution compares favourably with hydrogen. Presently over 80% of our energy needs are met from fossil fuels [1,2], with energy needs having grown tremendously since the industrial revolution: world wide energy consumption in 2001 was 13.5TW [2,3], in 2011 15TW [4], and this is forecast to grow to 27TW in 2050 [5] and 43TW by 2100 [4]. Present fossil fuel sources could supply 25-30TW annually for several centuries [6]. But $CO_2$ emissions from fossil fuel use are growing year-on-year, with 30Gt of carbon emitted in 2008 [7], giving an atmospheric concentration of 380ppm and forecasts of 700ppm by 2100 [8], under a business-as-usual scenario, where there is no change to energy supply and use. At a concentration of 550ppm, unavoidable climate change occurs and more than 10TW of carbon-free energy is needed simply to maintain this concentration [2]; a correspondingly larger proportion of carbon free energy is required to reduce the $CO_2$ concentration.

The following problems are of global concern:

- The confluence of peak oil production, finite and declining fossil fuel supplies, the cheap price of coal (external costs are not included in the \$0.03/kWh price [2]) and the inexorably rising cost of fossil fuels as a result of perceived shortages and geopolitics.

- Environmental destruction as a result of fossil fuel extraction via oil wells and rigs and fracking. The burning of fossil fuels emits unburnt hydrocarbons and aromatics, $NO_x$ and sulphur oxides, contributing to pollution and health issues, e.g. asthma.
- Many chemicals, e.g. plastics and fertilisers are synthesised from fossil fuels. Chemical processes require an energy input that comes from fossil fuels, but will have to come from renewables in the future.

Anthropocentric emissions of $CO_2$ into the atmosphere have lead to a carbon concentration of 399 ppm (2015), which is approaching the point where serious climate change will occur. We must also bear in mind that $CO_2$ emissions can take 30-40 years to have an impact. Thus, as a society, we are required to cut $CO_2$ emissions and try to use any $CO_2$ that may be produced.

The US Department of Energy has identified challenges in catalysis for sustainable energy and a priority to develop catalysts for photodriven conversion of $CO_2$ and $H_2O$ to fuels [9]. Europe has an aim to have 20 % renewable energy by 2020 and a 20% reduction in energy use [10]. The European Renewable Heating and Cooling and Photovoltaics Technology Platforms [11] have been established to drive policy in this area. Another perspective, given the subject of this Special Issue of Advanced Materials, are the Irish Government's Department of Communications, Energy and Natural Resources' 2007 Energy White Paper [12] and the 2010 Renewable Energy Plan [13], plan to have 30–40% of Ireland's electricity produced from renewables by 2020; natural gas will provide 50% and oil and coal will be a tiny contribution. Thus, policy makers have identified responses to the problems of fossil fuel supply and $CO_2$ emissions and the technology to enable this progress needs to be developed.

There will not be a single solution to securing the future energy supply, in the way that fossil fuels have dominated for the past 120 years. Rather, a number of solutions, depending on the problem and the location, will be pursued and will exploit some form of renewable energy [14]; solar energy is the most globally suitable energy source. In one hour 12 TW of solar power hits the earth, which is similar to the present energy use of the planet in one year. Of the

120,000 TW/year of solar insolation [15], around 600 TW/year is useful [2,3], which is 20 times predicted world demand for 2050 [16]. However, despite its potential availability, solar is anisotropically spread over the planet and suffers from diurnal variations. Using concentrators and storing solar energy in the form of chemical bonds, i.e. fuels, will mitigate against the disadvantages.

In the remainder of this Special Issue Progress Review, **Section 1.2** introduces some concepts in photocatalysis, with references to earlier reviews provided for readers interested in more detail, **Section 2** briefly outlines some pitfalls of modelling substitutional $TiO_2$ doping using density functional theory (DFT) and highlighting where blind application of DFT can result in erroneous interpretations. **Section 3** introduces some early experimental work on surface modification of $TiO_2$ with metal oxides. **Section 4** summarises our work on a series of metal oxide nanocluster modified rutile and anatase systems and **Section 5** discusses comparisons with the growing body of experimental work on these systems. S**ection 6** provides a perspective with the aim to devise general insights that will help in designing the next generation of $TiO_2$ photocatalysts. **Section 7** is a short summary of this progress report.

### 1.2 A Brief Introduction to Photocatalysis

Thus in securing a sustainable, reliable and secure energy supply, at reasonable cost we aim to harvest solar energy to produce useful fuels which store energy in their chemical bonds. Two particularly exciting avenues in this regard are splitting of water into hydrogen for the impending hydrogen economy (using fuel cells) and the conversion of $CO_2$ that is emitted from burning fossil fuels into more useful fuels. This would, in principle at least, reduce greenhouse gas emissions as the emitted $CO_2$ from, e.g. a power station, would be captured and converted into fuels, giving a closed carbon neutral cycle.

There then arises the question of finding a technology to produce hydrogen from water or reduce $CO_2$ to useful fuels, using solar energy and cost-effective, abundant, safe, environmentally friendly and stable materials. Photocatalysis is one of the leading technologies to enable solar fuel production and has been extensively reviewed in e.g. refs [17-28]. Figure 1 shows a schematic of the principle of photocatalysis. Briefly, a semiconductor absorbs light of an energy determined by the photocatalyst band gap. The excited electrons and the valence band holes are then able to participate in chemical reactions: holes will oxidise molecules (water to hydroxyls or oxygen, organics to $CO_2$ and water), while electrons will reduce molecules ($CO_2$ to methane, oxygen to superoxide or reactive oxygen species).

Key requirements for visible light activated photocatalysts, which we will discuss throughout this Report, include: the photocatalyst will absorb visible light to maximise use of the solar spectrum, which peaks in the visible region, and the electrons and holes will migrate to reactive sites instead of recombining with each other, which results in production of heat or emission of light (luminesence); in either case, recombination reduces the activity of the photocatalyst. The photocatalyst should also use materials that are abundant, cheap, non-toxic, and stable in different environments.

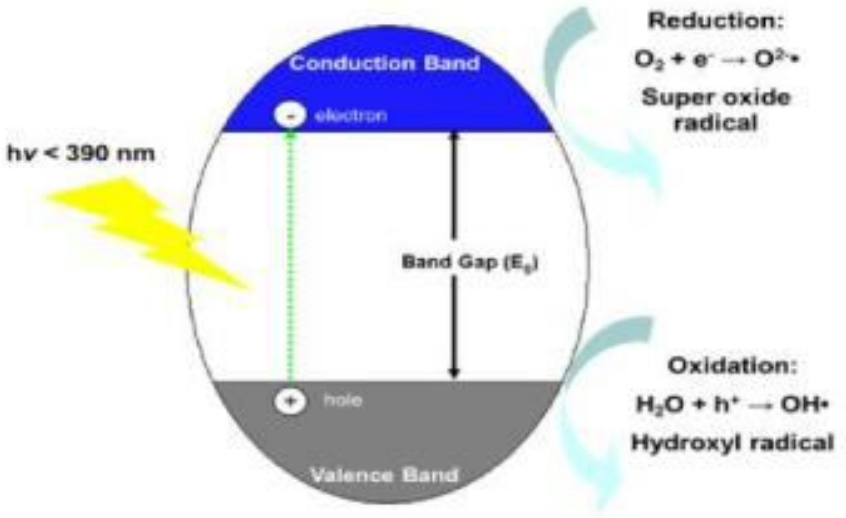

**Figure 1:** Schematic cartoon of the processes involved in photocatalysis

$TiO_2$ is the paradigm photocatalyst with many papers devoted to its properties as a photocatalyst. It absorbs UV light, with band gaps of 3 eV for the rutile phase and 3.2 eV for the anatase phase. Thus, much research has been performed to discover approaches to induce visible light absorption in $TiO_2$ and a selection of reviews from the extensive literature on $TiO_2$ photocatalysis can be found in Refs. [17-28]. However, a problem is that if $TiO_2$ can be made visible-light active, this activity tends to be much smaller than the UV-activity, while also reducing UV-activity. Thus the balance to be achieved is imparting a high level of visible-light activity but without reducing UV-light activity.

Since the pioneering work of Asahi et al in 2001 [29] there has been significant work devoted to studying substitutional doping of $TiO_2$ to induce visible light absorption [19,21,26,30,31,32,33,34]; the majority of work on doping has been with metal cations and more recent work has been on non-metal anion doping[19,20,21,29,30,31]. Since 2009, doping with both cations and anions, so-called co-doping [19,20,32,33,34], has been well studied. Since doping of $TiO_2$ is not the focus of this Progress Report, interested readers can read refs [17 – 28] for detailed discussions of this broad area. For the purposes of this Report, we note that doping of $TiO_2$ with foreign cations and anions leads to the appearance of dopant-induced states in the valence to conduction band energy gap that can act as carrier recombination centres. This has the effect of reducing the photocatalyst efficiency, which is one of the major issues with doped $TiO_2$. There are also other practical problems that can be associated with doping, including reproducibility, stability and knowing if the dopant has been incorporated.

There are other important topics within $TiO_2$ photocatalysis which we can only briefly mention in this Report. These topics are oxygen vacancies and $Ti^{3+}$ in the photocatalytic activity, Transient Spectroscopy to study electron/hole dynamics, and photoluminescence and we describe these in what follows.

In recent years, the role of oxygen vacancies and $Ti^{3+}$ in the photocatalytic activity of $TiO_2$ has been of great interest [35-50]. These works have shown that the properties of $TiO_2$ that are key for applications in photocatalysis can be modulated by its defect disorder. Excess electrons introduced through, e.g. hydrogenation or oxygen vacancies can extend light absorption into the visible region (e.g. Black $TiO_2$) and determine the surface reactivity and adsorption of key adsorbates such as water, oxygen or $CO_2$ Vacancies can provide active sites to adsorb and dissociate molecules such as water. O vacancies and $Ti^{3+}$ can be introduced by thermal treatments without or with hydrogen, particle bombardment or under typical reaction conditions. The extended absorption range of defective $TiO_2$ arises from formation of $Ti^{3+}$ states that lie below the conduction band edge into which valence band electrons can be excited with visible light. The high concentration of $Ti^{3+}$ results in the formation of a continuum of electronic states below the conduction band, rather than localised states which are detrimental to the activity of $TiO_2$. Thus, this approach to modifying the light absorption characteristics of $TiO_2$ can allow extended light absorption to longer wavelength but without affecting activity.

While characterisation of $TiO_2$-based photocatalysts uses standard techniques such as UV-vis spectroscopy, valence band XPS, dye degradation insights into the dynamics of electrons and holes and defects can be obtained from Transient Absorption Spectroscopy (TAS) [51-55] and photoluminescence (PL) [56-58]. TAS provides high temporal resolution (*ca.* 100 fs) and permits the identification of transient species and is used to study the trapping dynamics of electrons and holes; measurements of the transient absorption spectra in the presence of electron (hole) scavengers allows the spectra of holes (electrons) to be measured. Unfortunately, this technique has not been applied to the types of photocatalyst materials covered in this Report and this is an area with great potential in going beyond UV-vis and XPS measurements in unravelling the effect of the nanocluster modifier on the photocatalytic properties of $TiO_2$.

PL is a process in which electrons in a material are excited to the empty conduction band states to generate holes in the valence band and electrons in the conduction band. The recombination of the electrons and holes then takes place and releases energy as radiation, that is, the luminesence emission of the material. If defects are present, with states in the band gap, the excited electron can transition to the defect state and then further transition to the valence band; these defects can be, e.g. oxygen vacancies and the PL emission wavelength is characteristic for each material. PL can therefore be used to study the effect of $TiO_2$ modifications on electron-hole recombination processes and some examples of this will be discussed in the following.

## 2. Density Functional Theory Simulations of $TiO_2$ Doping: Some Dangers

In developing $TiO_2$ based photocatalysts, DFT level simulations have been widely used to understand experimental results or to attempt to predict the properties of doped $TiO_2$ [21,29-34]. However, a simple blind application of DFT to doped oxides can yield less than reliable results and there is a strong need for researchers in this field to be careful with these simulations and this is discussed in the following examples.

Since the report of Asahi *et al.* on visible light photoactivity of N-doped $TiO_2$ [29], there has been a significant number of papers published using DFT simulations to study doped $TiO_2$ with the aim to understand systems with potential visible light activity. However, there are some important points that we must briefly discuss in this regard. The use of standard DFT-GGA (GGA) functionals to model the change in the band gap of $TiO_2$ with doping should be treated with extreme caution; adding the so-called +U correction [59,60] to GGA functionals (giving GGA+U) has been claimed to result in band gaps comparable to experiment for undoped rutile and anatase [61], but this correction should only be used to alleviate the self interaction error inherent in a GGA functional that causes incorrect delocalization of electrons

or holes in a metal oxide and not to open up the band gap (by imposing a large U value on Ti 3d states). So-called hybrid DFT, primarily the B3-LYP [62] and HSE [63] functionals, correct the band gap underestimation of GGA by mixing a portion of exact Hartree-Fock exchange with GGA exchange and correlation functionals. These functionals contain adjustable parameters, such as the exact exchange contribution that is usually set at 25 %. In the periodic plane wave basis set typical of the majority of publications in this area, they are significantly more expensive to run. In determining the position of defect states in the host oxide valence to conduction band energy gap, the magnitude of any band gap error plays a key role in the description of the defect states and their formation energies [64-66] and therefore results from DFT-level simulations need to be carefully considered, with comparisons to experiment or accurate computational approaches required to calibrate the reliability of these DFT results.

We have examined this issue in two particular cases – doping of rutile with trivalent dopants [67] and doping of rutile and anatase with tetravalent dopants [68] and we briefly describe some issues that arise with using different flavours of DFT to model doping of $TiO_2$.

In doping of rutile with trivalent dopants, Al, Ga and In are examples of this oxidation state. It is known that doping a metal oxide with a cation having a lower oxidation state results in formation of an oxygen hole since the dopant does not have enough electrons available to form $O^{2-}$ anions, as shown by extensive studies on paradigm systems of Li-doped MgO [69] and Al-doped $SiO_2$ [70]; the oxygen hole is a lattice oxygen with an O $2p^5$ configuration. Charge compensation, in which an oxygen vacancy forms to compensate the charge difference between Ti and two trivalent dopants is also important. This is well known in key technological materials such as Yittrum-stabilised $ZrO_2$ and Al-doped $TiO_2$.

We undertook a study of these issues using GGA-DFT, GGA+U and HSE06 to investigate Al, Ga and In doped rutile. In this work, we applied a Hubbard U to the Ti 3d states (U = 4.5 eV, commonly used) and to the O 2p states (U = 7 eV [69,70]) since refs [69, 70, 71] show that GGA-DFT cannot describe the nature of the oxygen hole state. Figure 2 summarises our results by

showing the local geometry around the dopant, the electronic density of states projected onto the O 2p states of $TiO_2$ and the excess spin density (which is the difference between the number of spin up and spin down electrons, which in this case is 1) for each dopant. Focussing on hole localisation and the resulting defect state, GGA delocalizes the hole over all oxygen in $TiO_2$, with no distortion to the atomic structure, and there is no electronic state in the valence-conduction band energy gap. This is typical of GGA for lower valent cation doping and arises from the tendency of LDA and GGA approximations to delocalize otherwise localized electronic states; incomplete cancellation of the electron self-interaction is the generally accepted origin of this fundamental failing of LDA and GGA functionals.

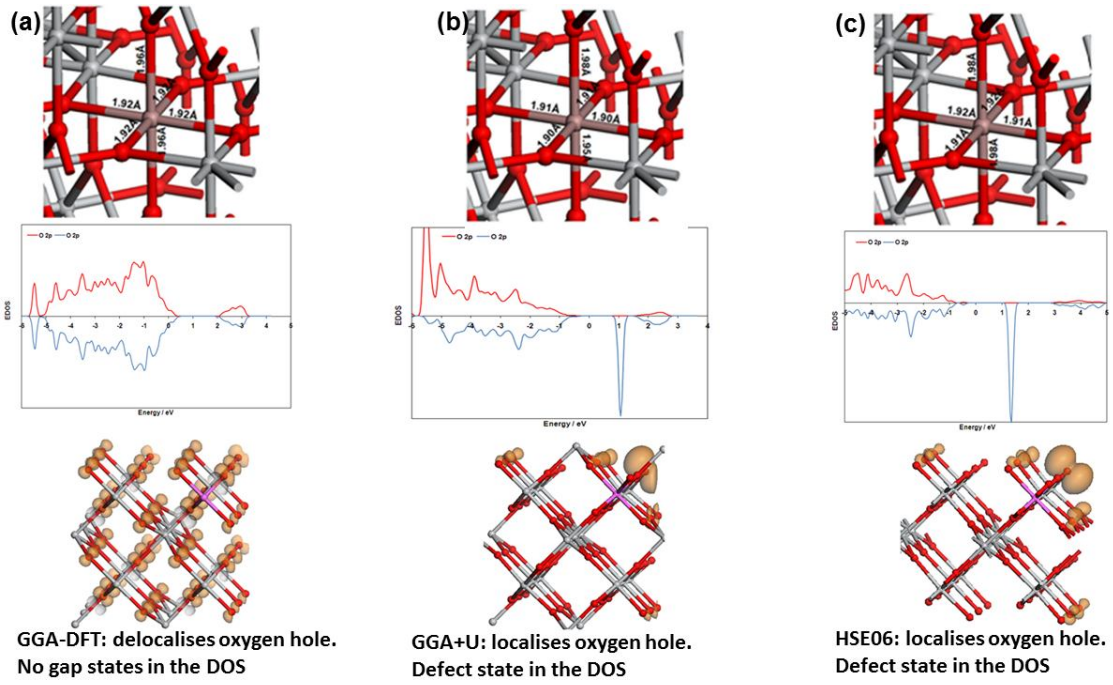


**Figure 2:** Atomic structure (top panels), Electronic density of states (PEDOS), projected onto O 2p states (middle panels) and excess spin density (bottom panels) for Al-doping of rutile $TiO_2$ from **(a):** GGA, **(b):** GGA+U and **(c):** HSE06 calculations. The PEDOS plots are spin polarised and the spin density isosurfaces enclose surfaces with volumes up to 0.02 eV / Å. Adapted from [67], 2013, Institute of Physics

By adding the +U correction to the O 2p states or using hybrid DFT (HSE06), this deficiency in GGA can be remedied. Both approaches localize the resulting hole state on a single oxygen atom, which results in a typical polaronic distortion of the local atomic geometry near the dopant, specifically an elongated metal-oxygen distance of 2.14 Å (GGA+U) and 2.15 Å (HSE06) for Al, 2.14 Å (GGA+U and HSE06) for Ga and 2.16 Å (GGA+U) and 2.15 Å (HSE06) for In respectively. In addition, GGA+U and HSE06 produce a localized defect state lying in the valence-conduction band energy gap, at 1.30/1.25/1.05 eV above the valence band edge for Al/Ga/In from GGA+U and 1.65/1/55/1.25 eV above the valence band edge for Al/Ga/In from HSE06.

**Table 1:** Formation energies of the compensating oxygen vacancy in Al, Ga and In doped bulk rutile $TiO_2$ from GGA+U and HSE06.

| Dopant | $E^{vac}$ / eV GGA+U | $E^{vac}$ / eV HSE06 |
|---|---|---|
| Al | +0.27 | -0.85 |
| Ga | +0.05 | -1.31 |
| In | -0.31 | -1.21 |

Thus, GGA+U appears to be suitable for consistently describing the structural and electronic properties of trivalent doped rutile. However, there are some questions about calculated energy differences when applying different DFT approaches, which in this case is the formation energy of the charge compensating oxygen vacancy to give the $2Al_{Ti} + V_O$ defect complex. **Table 1** shows the formation energies of the charge compensating oxygen vacancy from GGA+U and HSE06. The DFT approach affects the formation energies of compensating oxygen vacancies and one might incorrectly interpret the GGA+U result for Al-doped rutile to indicate that the compensating oxygen vacancy will not form, thus predicting an empty state

in the energy gap of rutile which could be interpreted as giving a red shift in light absorption. By contrast, HSE06 predicts correctly, when compared with experiment, O vacancy compensation which removes the dopant induced hole state in the VB-CB energy gap, and this particular doping strategy will not modify the absorption edge of $TiO_2$. Thus, extreme care must be taken when evaluating the stability of doped $TiO_2$ systems when using DFT, as incorrect interpretations can be developed, which can lead to erroneous predictions regarding and change to the VB-CB energy gap.

For tetravalent dopants, namely Zr and Ce, doping of $TiO_2$ results in no issues with charge compensation since these dopants have a +4 oxidation state. Comparing the DFT-GGA, GGA+U and HSE06 description of Zr doped bulk rutile and anatase, the different DFT methods give the same qualitative result. Zr-doping makes no modifications to the electron structure of $TiO_2$ since the empty states of $Zr^{4+}$ lie above the conduction band edge of $TiO_2$. The local structural distortions due to dopant incorporation are also consistently described with these DFT approaches.

However, when we consider Ce-doping of bulk $TiO_2$, there is a strong dependence on the choice of DFT approach, which is exemplified in **Figure 3**. We note firstly that the GGA+U set-up has no Hubbard U on Ce (there is only one Ce atom present so that delocalization of an electron over multiple Ce sites [72] is not possible). Figure 3 shows the atomic structure around the Ce dopant site and the Ti 3d and Ce 4f projected electronic density of states from GGA+U and HSE06. The local geometries around the dopant are essentially identical. The HSE06 density of states shows that the empty Ce 4f states lie above the bottom of the Ti 3d derived conduction band. Thus, there will be no band gap change in Ce doped bulk $TiO_2$. The GGA+U result, using the Hubbard U parameter set described above, gives a different interpretation, whereby a small reduction in the energy gap is predicted. Therefore, there is a clear disagreement between the two DFT approaches in describing the effect of Ce doping on the electronic structure of bulk $TiO_2$.

Furthermore, if we now consider other (reasonable) GGA+U parameter sets, e.g. applying U = 5 eV on Ce then the empty Ce 4f state lies at the energy of the CB edge which is more consistent with the HSE06 result. It is therefore unfortunately possible to tune the relative positions of the Ce 4f and Ti 3d states by using different values of the Hubbard U on Ti and Ce, which is of course an unsatisfactory situation and must be borne in mind when undertaking work on doping of $TiO_2$.

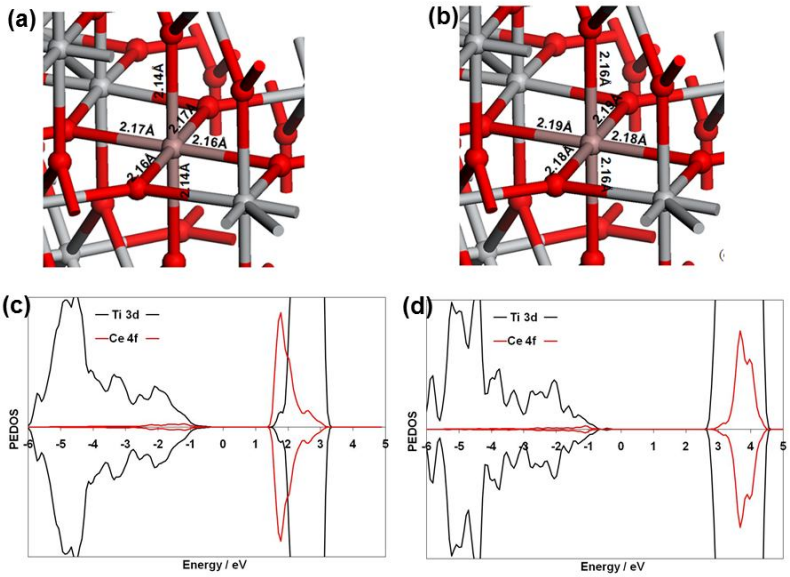


**Figure 3:** Atomic structure (top panels) and electronic density of states (PEDOS), projected onto Ti 3d and Ce 4f states (middle panels) for Ce-doping of rutile $TiO_2$ from **(a), (c)**: GGA+U, and **(b), (d):** HSE06 calculations. The PEDOS plots are spin polarised.

Adapted from [68], 2011, American Chemical Society

Since there can also be issues with experimental studies of doped $TiO_2$, alternative approaches to modify $TiO_2$ need to be explored and our approach beyond simple doping involves

modifying the surface of $TiO_2$ to achieve the requirements for visible light activated $TiO_2$ photocatalysts.

## 3. Surface Modification of $TiO_2$ with Metal Cations

Given the significant issues associated with doping of $TiO_2$, from both a modelling and experimental perspective, but at the same time the potential gains from developing a visible light activated photocatalyst, there is significant interest in exploiting other modifications of $TiO_2$ to induce visible light absorption, reduce charge recombination and enhance the reactivity towards molecules such as water or $CO_2$. Modification of $TiO_2$ with metal species, [17-21] or with nanoclusters of other metal oxides [73] provides an exciting route to meeting this aim.

The group of Hashimoto has presented valuable work studying the grafting of metal cations onto $TiO_2$ instead of doping with these metals. This group found efficient visible light-sensitive photocatalysts by grafting Cu(II) ions onto $TiO_2$ and $WO_3$ [74] and Cr(III)-grafted $TiO_2$ [75]. After preparation the modifiers were characterised as non-bulk oxides of the corresponding metal cations, namely CuO and $Cr_2O_3$. No bulk phases of either oxide were present, indicating very small surface adsorbed species were prepared. Visible light absorption was observed and explained as excitation of electrons from the $TiO_2$ valence band into CuO or $Cr_2O_3$ states lying below the conduction band of $TiO_2$. These electrons could then be transferred to molecules such as $O_2$ to drive chemical reactions. In addition, Cr(III)-grafting was compared with Cr(III) doping and the latter was much less efficient than the grafting process, indicating that modifying the surface of $TiO_2$ is potentially a better approach to induce visible light absorption than doping of $TiO_2$.

Our experimental collaborators in the group of Prof. Tada have developed the chemisorption-calcination cycle (CCC) technique, where metal complexes are adsorbed via chemical bonds

and the organic part is oxidized by post-heating, to prepare extremely small nanoclusters of oxides supported on $TiO_2$ [73, 76]. In this regard, **Figure 4** presents some key spectroscopic results from this experimental work [77,78], showing the effect of CuO modification on the electronic structure of $TiO_2$. Figure 4 (a) shows the UV-vis spectrum for CuO-modified $TiO_2$ as a function of CuO loading, while (b) shows a blown up portion of the UV-vis spectrum around the absorption edge. As the CuO loading increases there is a clear red shift in the absorption edge to longer wavelength, thus shifting light absorption into the visible region. In figure 4 (c) we show the valence band XPS spectrum that displays the change in the position of the VB edge as a function of CuO loading. It is clear that as the loading of CuO increase, the position of the VB edge shifts to higher energy (consistent with the red shift in light absorption), with a maximum shift of 0.7 eV. Closer inspection suggests two regimes of the VB shift – a lower CuO loading with small shifts and then an increase to significantly larger shifts at higher loading. It is possible that the VB-XPS data suggest an effect of loading on the mechanism of the red shift in the absorption edge of $TiO_2$. We will return to this system in Sections 2 and 3.

In figure 4 (d) and (e), we show the UV-vis and VB-XPS spectra for $FeO_x$-modified $TiO_2$ from ref. 77. The UV-vis spectrum shows the red shift of the absorption edge with increased $FeO_x$ loading on $TiO_2$, while the VB-XPS plots indicate an upwards shift of the VB edge with increased $FeO_x$ loading

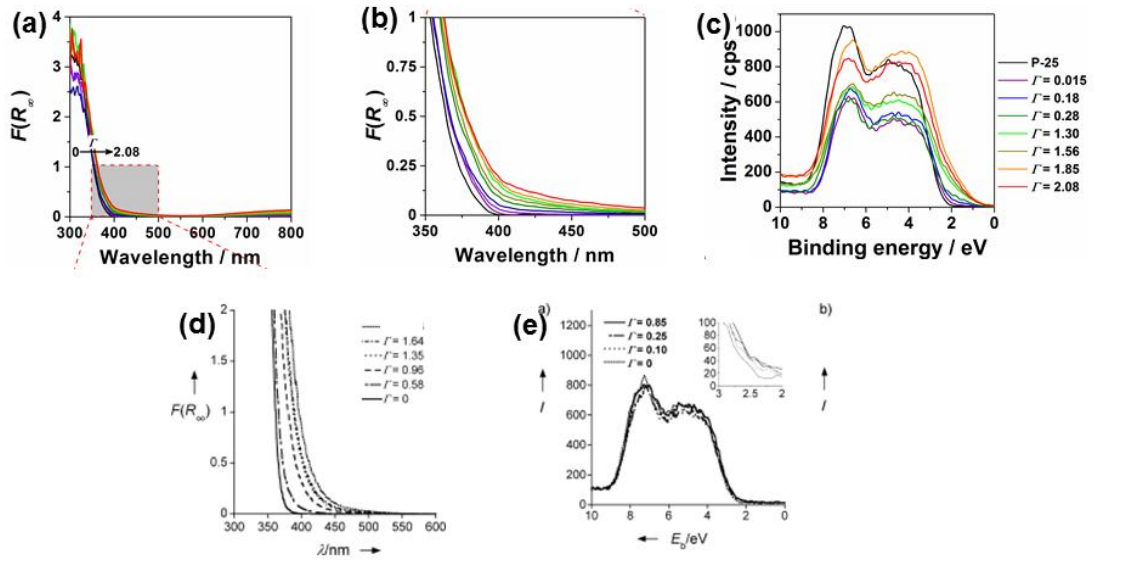


**Figure 4:** Experimental Results for **(a), (b), (c):** CuO-modified $TiO_2$ and **(d) and (e):** FeOx-modified $TiO_2$. (a): UV-vis spectrum for CuO-modified $TiO_2$ as a function of CuO loading (b) Inset of the UV-vis spectrum showing the shift of the absorption edge and (c) valence band XPS spectrum showing the change in the VB edge as a function of CuO loading.

(a), (b) and (c) Reproduced with permission from [78], 2013, American Chemical Society

(d) and (e) Reproduced with permission from[77], 2011, Wiley

Thus, the work from the groups of Hashimoto and Tada show that the strategy of modifying $TiO_2$ with metal oxide nanostructures has potential to meet some of the outlined requirements for a visible light active photocatalyst, while addressing the issues encountered by $TiO_2$ doping or by instability in, e.g. CdS-modified $TiO_2$. In order to advance this novel route to developing new photocatalyst materials, density functional theory simulations are a key tool to both understand experimentally characterized systems and develop new materials systems with the necessary properties to enable visible light activated photocatalysts.

In our work on surface modified $TiO_2$ photocatalysts, we have used first principles DFT simulations to describe how modifying $TiO_2$ rutile and anatase surfaces with metal oxide nanoclusters (NCs) can be used to develop potential photocatalysts with the properties

required for a photocatalyst material, while working together with experimentalists to confront the DFT predictions. The key properties our work has focused on include

(1) forming stable nanocluster modified $TiO_2$ structures – that is adsorbing the oxide clusters strongly at the surface so that they do not desorb or diffuse and aggregate into larger, less active particles or films. In a recent paper [79] we examined the energetics of $TiO_2$ cluster aggregation and found that although gas phase cluster aggregation to larger structures is favourable, the anchoring of the nanocluster on the $TiO_2$ surface actually disfavours nanocluster aggregation and indicates that these nanoclusters will be stable as isolated species.

(2) modifying the light absorption properties of $TiO_2$: that is shifting the absorption edge of $TiO_2$ to longer wavelength to capture more of the electromagnetic spectrum and exploit visible light to produce electrons and holes.

(3) use the surface modified structure and the nature of the nanocluster modifier to facilitate spatial separation of photogenerated electrons and holes which will be useful in reducing charge recombination

(4) increase reactivity towards molecules such as CO, $H_2O$ or $CO_2$. The nanostructure of the modifier may also be important here by making it easier to form, e.g. oxygen vacancies or provide active sites for molecular adsorption and dissociation, when compared to unmodified $TiO_2$, although this is an aspect that is currently being researched.

## 4. Surface Modification of $TiO_2$ for Visible Light Absorption: Materials Lead Design of Photocatalyst Materials

### 4.1 $TiO_2$ Nanocluster Modified Rutile $TiO_2$ as a Model System for Nanocluster Modification Induced Visible Light Absorption

In our work on surface modified $TiO_2$, we have chosen $TiO_2$ nanocluster-modified rutile (110) as our model system [79-81] to explore the many factors involved in devising photocatalysts that were outlined in the previous section. **Figure 5** shows the atomic structure of free and supported $TiO_2$ nanoclusters, ranging from a $Ti_2O_4$ "molecule" to a 1.5 nm diameter $Ti_{30}O_{60}$ nanocluster, that is approaching the diameter of metal oxide nanoclusters typically used in experimental work; work is ongoing in our group on modifying rutile and anatase surfaces with larger clusters, aiming for 3 – 4nm diameter structures.

Also shown in figure 5 is the adsorption energy, in eV, of the nanocluster at rutile (110); the adsorption energy is defined as

$E^{ads} = E\ (TiO_2NC—TiO_2) – [E(TiO_2\ NC)+ E(TiO_2)]$

Where $E\ (TiO_2NC—TiO_2)$ is the total energy of the $TiO_2NC$ modified rutile (110) surface, $E(TiO_2\ NC)$ is the total energy of the free nanocluster and $E(TiO_2)$ is the energy of the unmodified rutile (110) surface; the adsorption energy is therefore the energy gained when the nanocluster adsorbs at the surface compared to the reference of separated nanocluster and surface. All adsorption energies are negative, and the magnitudes of the adsorption energies indicate strong binding of the nanocluster at the rutile (110) surface. We further showed that when the nanoclusters are anchored at the surface it is not energetically favourable for them to aggregate into larger structures, which would then kill any advantaged gained by having the $TiO_2$ surface modified with the nanoclusters [79].

Upon examining the atomic structure of the free nanoclusters, we observe the presence of Ti and O species that are not found in bulk $TiO_2$ polymorphs. Of particular note are (1) singly coordinated *titanyl* oxygen, with Ti-O distances around 1.70 Å, significantly shorter than the Ti-O distances for 2-fold coordinated oxygen, and (2) three- and four-fold coordinated Ti species, which again are not found in bulk. Leaving aside the very smallest $TiO_2$ nanoclusters shown in figure 5, if we consider our 1.5 nm diameter nanocluster, with composition $Ti_{30}O_{60}$,

then at this cluster size there are still titanyl oxygen and 4-fold coordinated Ti sites present. These undercoordinated Ti species are key to further properties of these particular assemblies [81].

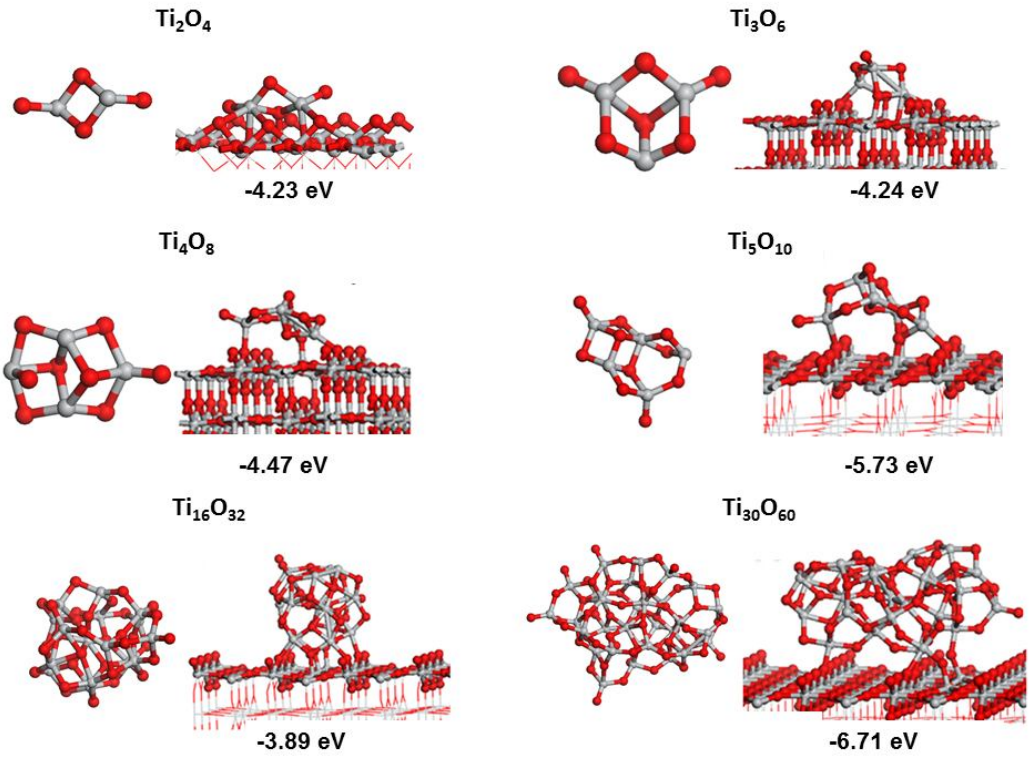


**Figure 5:** Atomic structure of a selection of free and supported (on rutile (110)) $TiO_2$ nanoclusters. Also shown under each supported nanocluster structure are the computed adsorption energies in eV.

Upon examining the atomic structure of supported nanoclusters, we find that there is some correlation between the magnitude of the adsorption energy and the number of new Ti-O bonds formed after relaxation: generally the more Ti-O bonds that can be formed between the nanocluster and the support (for a given nanocluster composition), the more negative is the adsorption energy. We also propose that the inability of the nanoclusters to aggregate stems from the formation of these new nanocluster-surface bonds, the breaking of which is required

for diffusion of the clusters over the surface to form the aggregates. After adsorption and relaxation, $TiO_2$ nanocluster binding can remove some titanyl oxygen (which bind to Ti atoms in the surface, e.g. $Ti_8O_{16}$), but for most clusters, there are still titanyl bonds present. In addition, 4-fold Ti species present in the free nanocluster can still persist in upon formation of the composite structure. A detailed discussion of the geometry in these composite structures is presented in refs [79-81].

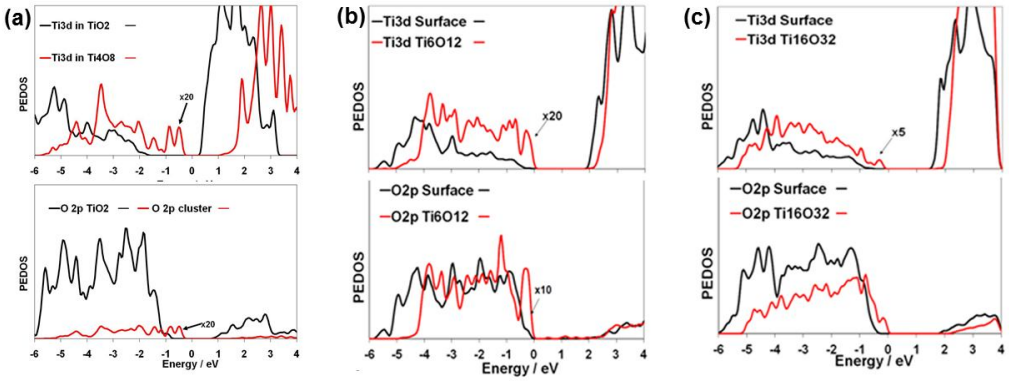


**Figure 6:** Electronic density of states projected onto Ti3d (top panel) and O 2p (bottom panel) states from a selection of $TiO_2$ nanocluster-rutile (110) composites. The zero of energy is the top of the highest occupied states and the nanocluster DOS are multiplied by the indicated factors to aid the reader.

(a) Reproduced from [80], 2011, The Royal Society of Chemistry

(b), (c) Reproduced from [79], 2013, The Royal Society of Chemistry

In terms of understanding photocatalytic properties of surface modified $TiO_2$, we next examine the projected electronic density of states (PEDOS) and the PEDOS for selected $TiO_2$ nanocluster-modified rutile systems is shown in **Figure 6**; this is a representative sample of compositions and PEDOS plots for all the $TiO_2$ nanocluster-modified rutile systems we have studied are presented in refs [79-81].

The PEDOS is plotted to show contributions from Ti 3d and O 2p states in the rutile surface (black lines) and the $TiO_2$ nanocluster (red lines) to allow the contributions of the nanocluster and the surface to the important electronic states around the valence and conduction band edges to be determined. The PEDOS plots show that there are new electronic states lying above the original valence band edge of rutile (110) and that these states are derived from the $TiO_2$ nanocluster. The consequence of this is that the valence band edge of the $TiO_2$ nanocluster-modified rutile system will be pushed higher in energy and this will then allow absorption of photons of lower energy, thus inducing a red shift in the absorption edge and push light absorption towards the visible region of the electromagnetic spectrum. The size of the shift of the VB edge upon nanocluster modification depends on the size/composition of the $TiO_2$ nanocluster – but we find large shifts of up to 1 eV from this simple PEDOS analysis. In identifying the origin of the new nanocluster-derived states we find that the low coordinated oxygen atoms in the nanocluster dominate these new electronic states.

Of course, these calculations use the so-called GGA+U approach, which is applied to describe correctly reduced $Ti^{3+}$ states that can be present as a result of photoexcitation or reduction of the material. Although GGA+U can give a partial widening of the valence to conduction band energy gap compared to a GGA functional, the energy gap remains underestimated compared to experiment. At present a hybrid DFT calculation of these structures, with a more reliable energy gap, is not feasible within a plane wave basis set approach. However, we shall see in the next sub-sections that the trends found from the GGA+U calculations are consistent with experimental results on similar systems, giving some confidence in the qualitative results regarding the effect of nanocluster modification on the $TiO_2$ energy gap.

The next key requirement for the photocatalyst material is the fate of the electrons and holes produced by light absorption. Ideally, the structure of the potential photocatalyst should prevent easy recombination of the photogenerated electrons and holes and devising structures that may trap or localize electrons and holes in particular sites can be beneficial in this regard.

The low coordinated atomic sites described for these nanoclusters may be such sites and we investigate the localisation of photogenerated electrons and holes in our model $TiO_2$ nanocluster modified rutile systems.

These calculations use a simple model whereby a triplet electronic state is imposed on the system and this has the consequence that a previously empty Ti 3d state is now occupied and there is a hole in the valence band. Therefore, a photoexcited electron and hole are present and the system relaxes to the lowest energy electronic state within a triplet spin configuration which is a crude, but useful, model of the photoexcited state. We have studied where the electron and hole prefer to localize and some interesting energies that can be extracted. These energies are the following

(1) The vertical singlet-triplet energy which corresponds quite well to the simple valence to conduction band energy gap from the PEDOS; the triplet state is not allowed to relax (so that it takes the singlet ground state geometry)

(2) The relaxed singlet-triplet energy in which the triplet state is allowed to relax in response to the promotion of an electron to the conduction band.

The energy difference between the ground state energy and the relaxed singlet-triplet energy approximates the excitation energy, while the energy difference between the unrelaxed and relaxed triplet electronic states is the relaxation or trapping energy, related to the energy gained when the geometry relaxes to allow the electron and hole form polaron states. Di Valentin and Selloni described this model for anatase [82] (see also refs [83,84]) and we have used it extensively in understanding different modifications of $TiO_2$ with nanoclusters [81,85-87].

**Figure 7** shows the spin density from the relaxed triplet state for a selection of free and supported $TiO_2$ nanoclusters; ref [81] shows a more extensive set of nanoclusters and see also ref [88] for high level DFT results on electron-hole localisation in $TiO_2$ nanoclusters, showing consistency between the different DFT approaches and models.

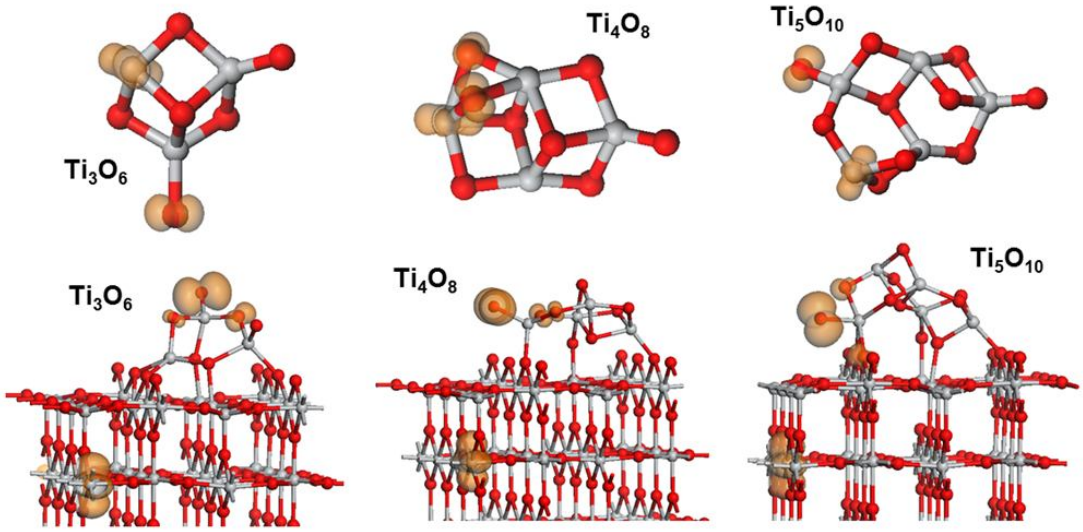


**Figure 7:** Excess spin density for a selection of free (top panel) and supported $TiO_2$ nanoclusters to show the location of photoexcited electrons and valence band holes. The composition of the nanocluster is shown beside each image. Isosurfaces enclose spin densities up to 0.02 eV / Å.

Reproduced from [81], 2014, American Chemical Society

In the relaxed triplet state, the spin density shows strong localisation of the photoexcited electron and hole. In the free nanoclusters, the electron always localises on a Ti site with the lowest coordination in that particular nanocluster: in these sample nanoclusters, this is always a 3-fold coordinated Ti site (for larger nanoclusters, it is a 4-fold coordinated Ti site). The computed Bader charge on these sites is *ca.* 1.65 electrons, compared to 1.3 electrons for $Ti^{4+}$ sites, and the corresponding spin magnetisation is 0.95 electrons (it is smaller than 0.01 electrons for all other Ti sites). There are consistent with the presence of a reduced $Ti^{3+}$ species. The $Ti^{3+}$-O distances are elongated by *ca.* 0.1 Å.

Considering the oxygen hole, Figure 7 shows the hole is strongly localised for all nanoclusters and the site for oxygen localisation is a terminal titanyl oxygen. In the $Ti_4O_8$ nanocluster, the oxygen hole is spread over two two-fold coordinated oxygen atoms, but we note that this hole

distribution was also found using very accurate time dependent DFT calculations [88]. It is clear that the oxygen hole is strongly localised in free $TiO_2$ nanoclusters. The computed Bader charge on the oxygen atoms carrying the hole is 6.8 electrons (7.3 electrons for lattice oxygen) and the computed spin magnetisations are *ca*. 0.85 electrons (spin magnetizations are smaller than 0.05 electrons on other oxygen atoms). The $Ti^{4+}$-$O^-$ distances in the nanoclusters are elongated by 0.1 – 0.12 Å over the $Ti^{4+}$-$O^{2-}$ distances, all of which are consistent with formation of a localised oxygen hole polaron.

For supported nanoclusters on the rutile surface, the electron localizes onto a Ti atom in rutile, reducing this Ti atom to $Ti^{3+}$. The computed Bader charge is 1.8 electrons and the spin magnetisation is 0.95 electrons. The oxygen hole always localises onto a low coordinated oxygen in the $TiO_2$ nanocluster, which for these nanoclusters is a singly coordinated terminal (titanyl) oxygen atom in the nanocluster. This pattern of oxygen hole localisation onto oxygen with the lowest possible coordination is the same as described in the free nanoclusters. The computed Bader charge for the hole carrying oxygen is in the range of 6.65 – 6.70 electrons, depending on nanocluster size; the computed spin magnetization is *ca*. 0.80 electrons, confirming formation of a localisation oxygen hole. The $Ti^{4+}$-$O^-$ distances around the oxygen hole site are elongated by up to 0.2 Å over the $Ti^{4+}$-$O^{2-}$ distances, again consistent with the formation of a localised, oxygen hole species.

This pattern of electron and hole localisation is found for all nanocluster modified rutile composites we have studied and confirms the analysis from the PEDOS that the electron and hole will localise onto the rutile (110) surface and the $TiO_2$ nanocluster, respectively. The separation of the electron and hole is beneficial for the photocatalytic activity, as it inhibits charge recombination, in particular in comparison with unmodified rutile $TiO_2$.

**Table 2:** Vertical singlet-triplet energy difference ($E^{vertical}$), the relaxed singlet-triplet energy difference ($E^{S-T}$) and the relaxation energy ($E^{relax}$) for nanocluster-modified rutile (110) structures and unmodified rutile (110) as reference.

| **Modified $TiO_2$ Structure** | $E^{vertical}$ / eV | $E^{S-T}$/ eV | $E^{relax}$ / eV |
|---|---|---|---|
| Unmodified Rutile (110) | 2.21 | 1.69 | 0.52 |
| $Ti_3O_6$-modified Rutile (110) | 1.61 | 0.25 | 1.37 |
| $Ti_4O_8$-modified Rutile (110) | 1.95 | 0.71 | 1.24 |
| $Ti_5O_{10}$-modified Rutile (110) | 2.09 | 0.59 | 1.50 |

**Table 2** presents the vertical singlet-triplet energy, the relaxed singlet-triplet energy and the relaxation energy for some nanocluster-modified rutile (110) structures along with the unmodified rutile (110) surface. The vertical energy difference shows the same trend as the simple VB-CB energy difference from the PEDOS: all nanocluster modified structures show a reduction in the vertical energy compared to unmodified rutile (110) and the magnitude of the reduction is dependent on the size of the $TiO_2$ nanocluster.

The relaxed singlet-triplet energies are also reduced compared to unmodified rutile (110), demonstrating that surface modification with $TiO_2$ nanoclusters induces a red shift in the wavelength of light absorbed. While a hybrid DFT level calculation of these energies would give a more precise indication of the change in the singlet-triplet energy, such calculations are presently not possible within a plane wave basis for these systems.

The relaxation energies for the nanocluster-modified $TiO_2$ structures are larger than for the bare surface which arises since the nanoclusters can undergo stronger relaxations upon formation of localised electrons and holes when compared with the $TiO_2$ surface.

### 4.2 Transition Metal Oxide Modified $TiO_2$: CuO and $FeO_x$ Nanocluster Modification to Induce Visible Light Absorption

Our experimental collaborators in the group of Prof. Tada have presented studies of $TiO_2$ modified with CuO [78] and FeOx [77] nanoclusters; a short summary of some findings was presented in **Section 3**. We have used our DFT simulation to examine the effect of these nanocluster modifications on the key properties for their use as a photocatalyst. Other combined experimental and DFT studies on transition metal oxide modified $TiO_2$ can be found in refs. [89-91] and will be discussed in Section 4.

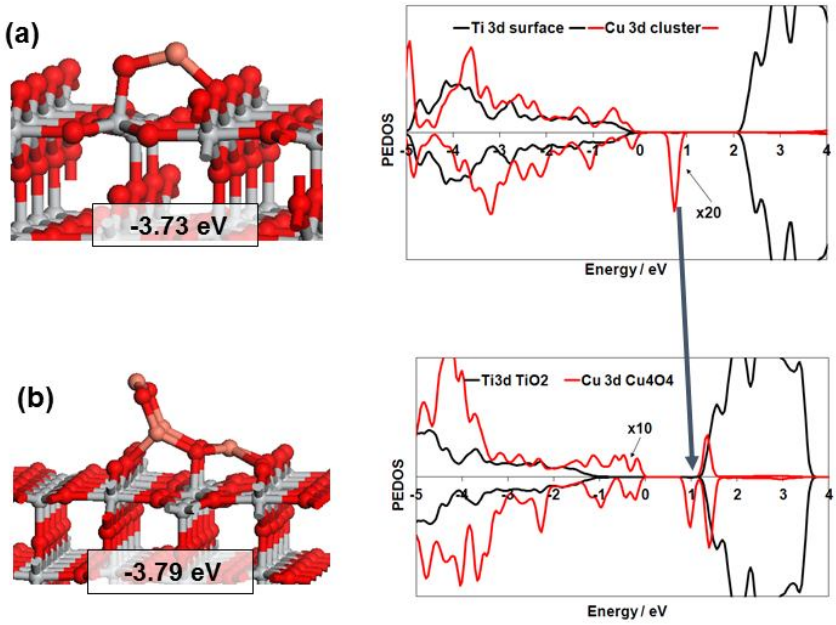


**Figure 8:** Atomic structure, computed adsorption energies and projected electronic density of states (PEDOS), projected onto Ti 3d, and Cu 3d states for **(a):** CuO-modified rutile (110) and **(b):** $Cu_4O_4$-modified rutile (110). The PEDOS plots are spin polarised and the zero of energy is the highest occupied electronic state. The arrow shows the position of the empty Cu 3d state in the two structures.

Reproduced from [78], 2013, American Chemical Society

**Figure 8** shows the atomic structure and PEDOS for rutile (110) modified with CuO nanoclusters with two representative compositions, namely CuO and $Cu_4O_4$. On rutile (110), the computed adsorption energies show strong adsorption of the CuO nanoclusters and this is driven by formation of interfacial Cu-O and Ti-O bonds between the nanoclusters and the surface. The CuO nanocluster has a Cu-O distance of 1.79 Å to the bridging surface oxygen and a Cu-O distance of 1.76 Å in the nanocluster. A 5-fold coordinated surface Ti binds to oxygen in the nanocluster, with a distance of 1.87 Å. The adsorbed $Cu_4O_4$ nanocluster displays bonding between three Cu atoms in the nanocluster and 2-fold bridging oxygen atoms in the surface. The Cu-O distances to the surface are 1.95, 1.96 and 2.1 Å. 5-fold coordinated surface Ti atoms bind to two oxygen atoms of the nanocluster, giving Ti-O distances of 1.91 Å. In the adsorbed nanocluster Cu-O distances lie in the range of 1.73 to 1.95 Å.

Figure 8 also shows the PEDOS for CuO nanocluster-modified rutile. The PEDOS show that CuO nanocluster modification of rutile surfaces can cause a significant change in the electronic structure around the valence and conduction band edges that depends, in the DFT studies, on the size of the nanocluster, which corresponds to the loading of CuO on the modified $TiO_2$ surface.

For modification of rutile with a CuO nanocluster a new, empty Cu 3d state is present in the VB-CB gap, which arises from the presence of a $Cu^{2+}$ oxidation state, with a $3d^9$ electronic configuration. We would therefore expect excitation of an electron from the $TiO_2$ derived valence band into the empty Cu 3d states below the $TiO_2$ conduction band edge, shifting light absorption to lower energy, consistent with the interpretation of Hashimoto and co-workers [74]. If we now consider the impact of the CuO nanocluster size (or loading) on rutile (110), there is some interesting behavior. Upon increasing the size of the CuO nanocluster, there is a significant upwards shift in the top of VB, which is *ca.* 0.7 eV for $Cu_4O_4$-modified rutile (110). The origin of this is the CuO derived occupied states that are found at higher energy

than the surface VB edge. At the same time, the empty $Cu^{2+}$ states, previously in the energy gap, are shifted upwards in energy to approach the $TiO_2$ CB minimum. Preliminary results on larger CuO nanoclusters place the empty Cu 3d states above the conduction band edge of $TiO_2$.

Thus, while there is a narrowing of the band gap compared to unmodified $TiO_2$, the origin of the band gap narrowing depends on the CuO loading. Given this apparent CuO loading dependence of the band gap change in CuO-modified $TiO_2$, there is an interesting possibility that control of CuO loading could be a useful tool to tune the mechanism of the band gap reduction. This will then determine the nature of the photoexcited state, which in turn will determine the activity of the photogenerated electrons and holes for reduction or oxidation reactions.

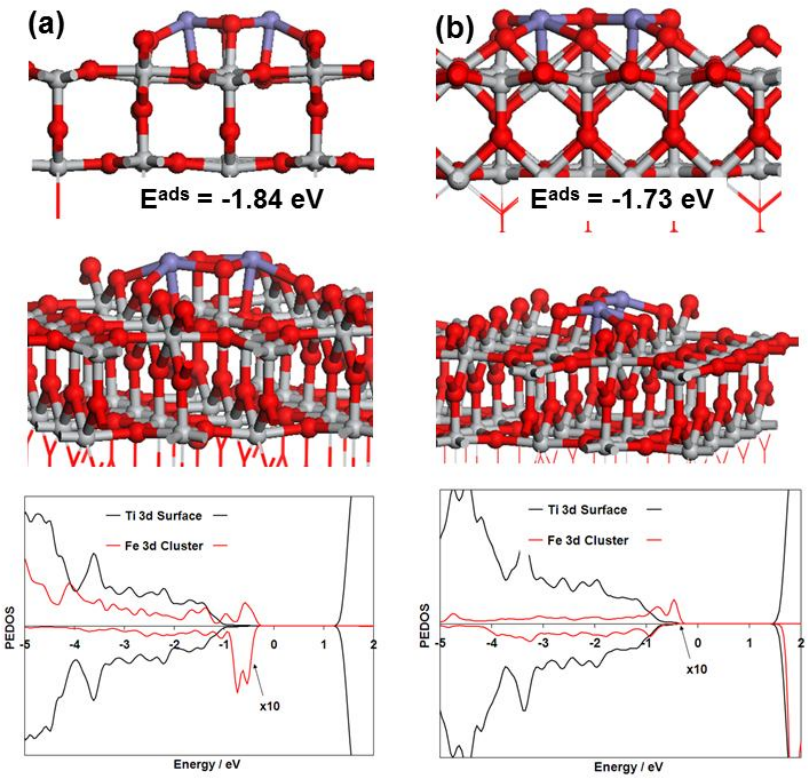


**Figure 9:** Atomic structure, computed adsorption energies and electronic density of states (PEDOS), projected onto Ti 3d, and Fe 3d states for (a): FeO-modified rutile (110) and (b):

$Fe_2O_3$-modified rutile (110). The PEDOS plots are spin polarised and the zero of energy is the highest occupied electronic state.

Reproduced from [92], 2011, The PCCP Owner Societies

We have also studied the effect of FeOx nanocluster (with $Fe^{2+}$ and $Fe^{3+}$ oxidation states) modification of rutile (110) [92], which was motivated by the work from Tada et al [77], as summarised in section 2, and Libera et al.[93] who also studied $FeO_x$-modified $TiO_2$ grown by ALD and characterised both visible light absorption and enhanced photocatalytic activity over unmodified $TiO_2$. Here, we summarise our simulation results on these systems, which facilitated an atomic level understanding of this interesting photocatalyst material.

**Figure 9** shows the relaxed atomic structure and computed adsorption energies (referenced to bare rutile (110) and free $FeO_x$) for modification of rutile (110) with $Fe_2O_2$ and $Fe_2O_3$ nanoclusters. The computed adsorption energies in figure 9 show that adsorbed iron oxide nanoclusters are stable and the magnitude of the adsorption energy indicates that the adsorbed nanoclusters should also be thermally stable.

The most stable adsorption structure of $Fe_2O_3$, has the O and Fe atoms in iron oxide arranged in a typical zig-zag pattern (O-Fe-O-Fe-O) observed in stable gas phase structures of $M_2O_3$ nanoclusters. The oxygen atoms interact with a 5-fold coordinated Ti atom in the surface,. Fe-O distances in the nanocluster are 1.82 Å and 1.93 Å, and the Fe-O distances to surface oxygen are in the range 2.02 - 2.09 Å. Ti-O distances to oxygen in the $Fe_2O_3$ nanocluster are in the range 2.1 - 2.2 Å. In $Fe_2O_2$, the Fe cations are bound to two bridging oxygen on rutile (110), with Fe-O distances of 2.11, 2.29 Å. Oxygen from $Fe_2O_2$ binds to a 5-fold coordinated surface Ti atom, with a Ti-O distance of 1.89 Å and the Fe-O distances in the iron oxide cluster are 2.04 and 2.12 Å.

In PEDOS plots of FeOx adsorbed at $TiO_2$, shown in figure 9, adsorption of the nanocluster results in the formation of new electronic states lying above the original rutile (110) valance

band edge. These states are derived from adsorbed FeOx nanoclusters. Therefore, adsorption of iron oxide at the rutile (110) surface pushes the top of the valence band to higher energy. The bottom of the conduction band is dominated by the empty Ti 3d states originating from the rutile surface. Thus, the interaction between iron oxide nanoclusters and $TiO_2$ is that the band gap of the composite structure will be narrowed compared to unmodified $TiO_2$; this gives a red shift in light absorption; we predict a shift of around 0.3 eV that suggests visible light absorption is possible.

Finally, the relative positions of the FeOx and rutile (110) electronic bands will facilitate charge separation after light absorption: excited electrons will be found on the $TiO_2$ support and the valence band holes will be found on the iron oxide nanocluster. Electrons and holes will therefore be spatially separated, reducing the possibility of electron-hole recombination.

### 4.3 $SnO_x$ and $PbO_x$-modified $TiO_2$: Exploiting the Steroechemical Lone Pair in $Sn^{2+}$ and $Pb^{2+}$ to Induce Visible Light Absorption

In choosing metal oxide modifiers of $TiO_2$, it is interesting to consider metals with two oxidation states, which give very different properties in the corresponding bulk oxides, and to examine if this allows tuning of both the magnitude of the red shift and the mechanism of the shift, simply by changing the oxidation state of the metal oxide modifier. An early work in this regard is from Boppana and Lobo [94] in which $ZnGa_2O_4$ was modified by SnO and $SnO_2$, which is achieved by using SnOx precursors with the desired oxidation state. SnO-modified $ZnGa_2O_4$ did have SnO and $SnO_2$ present, but not all SnO was oxidised; $SnO_2$-modified $ZnGa_2O_4$ had only $SnO_2$ present. The most striking result is that modification by SnO lead to a red shift in the absorption edge but modification with $SnO_2$ had no effect and therefore there is some effect due to the difference in the Sn oxidation states.

In this work we have examined modification of anatase, choosing the anatase (001) surface as a model of this form of $TiO_2$. While we recognise that (101) is the dominant surface, there has been significant interest in the less stable (001) surface of anatase [95-101] as it is considered more active for photocatalysis than the dominant (101) surface and therefore there has been significant effort devoted to devising routes to prepare materials with dominant (001) facets. In our work we use the unreconstructed, non-defective (001) anatase surface as our model.

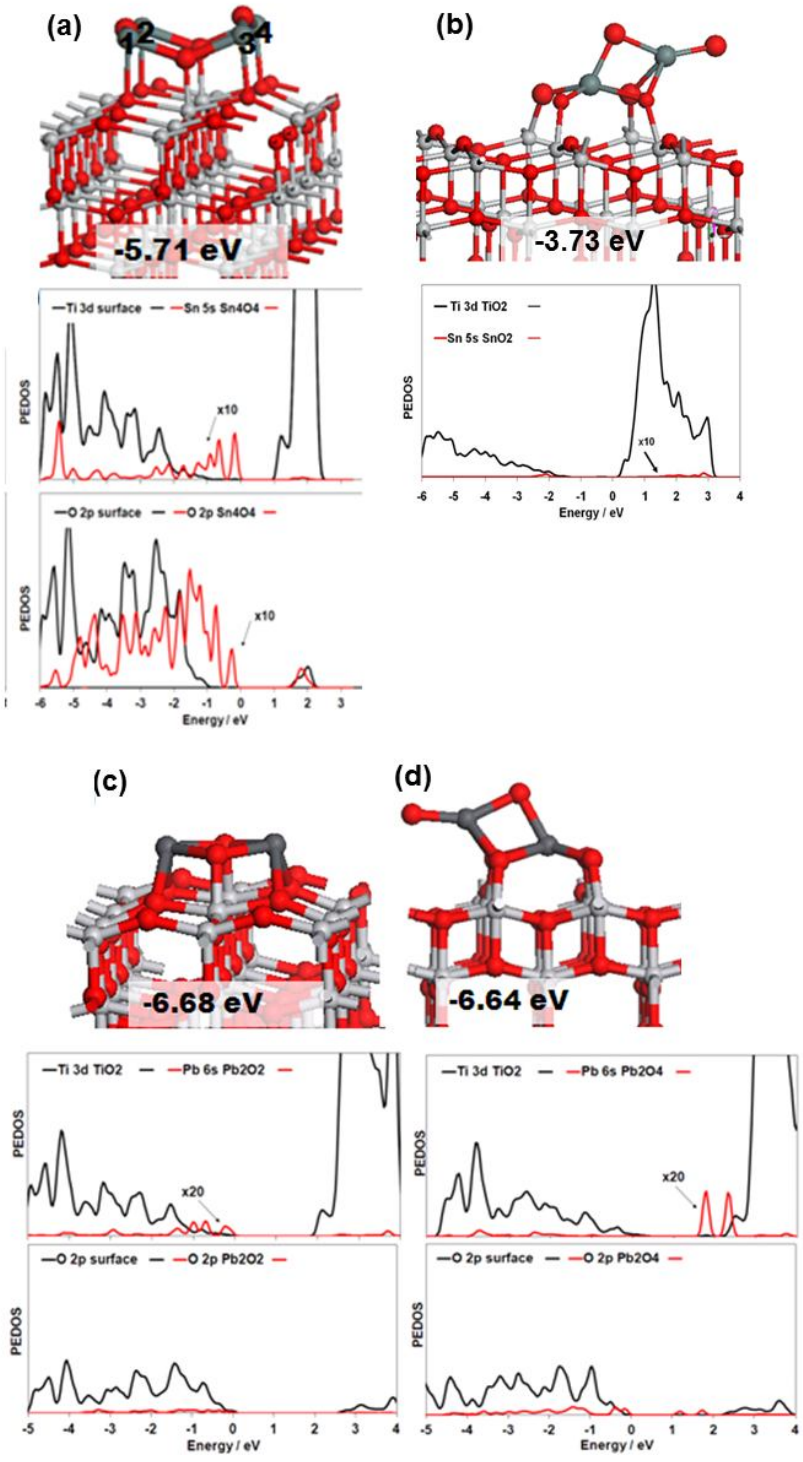


**Figure 10: (a):** Atomic structure, computed adsorption energies and Ti 3d/Sn 5s/O 2p PEDOS for SnO-modified anatase (001), **(b):** Atomic structure and Ti 3d/Sn 5s/O 2p PEDOS for $SnO_2$-modified anatase (001), **(c):** Atomic structure and Ti 3d/Pb 6s/O 2p PEDOS for PbO-modified anatase (001), **(d):** Atomic structure and Ti 3d/Pb 6s/O 2p PEDOS for $PbO_2$-

modified anatase (001). Also shown in the structure images are the computed adsorption energies.

(a), (b): reproduced from [86], 2013, The Royal Society of Chemistry

(c), (d): reproduced from [87], 2013, The Royal Society of Chemistry

We have investigated in this phenomenon in detail through two examples [86.87] and experimental data is also available to support our findings [90,91,102,103]. The oxide modifiers are (1) $SnO/SnO_2$ and (2) $PbO/PbO_2$; Sn and Pb can take +2 or +4 oxidation states with the former having an $s^2p^2$ electronic configuration. The +2 oxidation state of Sn and Pb is involved in the stereochemical lone pair in bulk SnO and PbO. These are characterised by a distorted atomic structure that has been described in detail over the last decade [104,105]

**Figure 10** summarises our results for $SnO/SnO_2$ and $PbO/PbO_2$ modified anatase (001); detailed results for other SnOx and $PbO_x$ nanoclusters on anatase and rutile are described in refs.[86,87,90,91]. All SnOx and PbOx nanoclusters adsorb strongly at the anatase (001) surface with adsorption energies ranging from and -3.37 eV to -6.68 eV, that are indicative of a strong interaction between the nanoclusters and anatase (001). It is particularly interesting to see that oxygen atoms in the anatase (001) surface are displaced from their surface sites to allow for interaction with the $SnO_2$ and $PbO_2$ nanoclusters, whereas the SnO and PbO nanoclusters tend to lie in a flat adsorption configuration to maximise cluster to surface binding. For the example of the $Sn_2O_4$ cluster, the displaced surface oxygen and nanocluster oxygen are in similar bonding environments; the surface oxygen atoms have been displaced by 1.11 Å and Sn-O distances are 2.10 - 2.15 Å. These are similar to Sn-O distances in SnO litharge (2.26 Å) and $Sn_2TiO_4$ (2.09 and 2.21 Å). PbOx nanoclusters show similar adsorption structures to

SnOx nanoclusters, with oxygen from the anatase surface migrating to interact with the $PbO_2$ nanocluster.

The most significant effect of the Sn and Pb oxidation state is in the changes to the electronic structure of anatase upon modification with the corresponding nanoclusters. The PEDOS plots in figure 10 show the PEDOS projected onto Ti 3d, Sn/Pb 5s/6s and O 2p states for SnO, $SnO_2$, PbO and $PbO_2$ nanoclusters supported on anatase. The modification with $SnO_2$ nanoclusters results in no significant changes to the valance or conduction band edges; there is a small Sn 5s contribution above the bottom of the conduction band and an O 2p contribution from $SnO_2$ oxygen atoms around 1 eV below the valence band edge. Thus, modification with $SnO_2$ should result in no shift in the absorption edge compared to unmodified anatase.

The change in oxidation state to $Sn^{2+}$ has a significant effect on the electronic structure of $TiO_2$. Here, SnO-derived Sn 5s and O 2p states are present above the valence band edge of anatase; a red shift of around 0.6 eV is expected and this would shift light absorption into the visible region. The effect of the $Sn^{2+}$ oxidation state is to introduce states derived from the Sn 5s-O 2p interaction that are typical of $Sn^{2+}$ and are understood in terms of the stereochemical lone pair in SnO and related chalcogenide (SnS, SnSe) solids [105].

For PbO and $PbO_2$ nanocluster-modified $TiO_2$, the effect of the Pb oxidation state is quite striking. For PbO-modified anatase, there are new PbO derived Pb 6s and O 2p states present above the anatase valence band edge, similar to the SnO derived electronic states with the same origin. The presence of these states shifts light absorption to longer wavelength. By contrast when the $PbO_2$ nanocluster is adsorbed at anatase (001) or rutile (110), there is also a band gap reduction, but this arises from a different mechanism: we find unoccupied Pb 6s states lying below the empty Ti 3d conduction band states of anatase so that the CB edge is now lowered in energy to give the band gap reduction.

### 4.4 ZnX (X = O, S, Se) Modified $TiO_2$: Controlling the Red Shift by the Choice of Anion

Metal oxide nanocluster modified $TiO_2$ has obviously been the primary focus of our work and this review. Going beyond oxide nanocluster modifiers, in recent work, we have studied the effect of changing the anion in the modifier to other chalcogenides elements, that is the series O, S and Se. In, e.g. the SnX series (X = O, S, Se, Te) there is a very interesting phenomenon whereby the bulk crystal structure changes from distorted litharge (SnO) to a rock salt structure (SnSe) which is determined by the relative energy of the Sn 5s/5p and anion n*p* states. In another example, the identity of the anion in ZnO, ZnS and ZnSe changes the size of the band gap and this may be useful for modifying the $TiO_2$ valance to conduction band energy gap by modification with this series of nanoclusters.

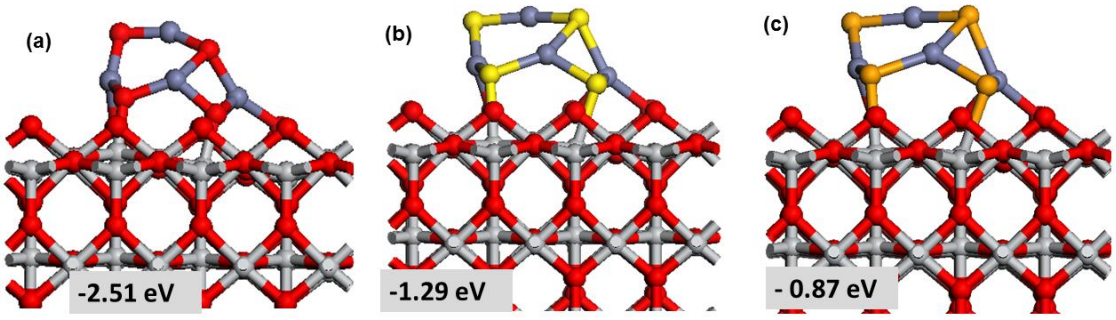


**Figure 11:** Atomic Structure and computed adsorption energies in eV, of **(a):** ZnO-, **(b):** ZnS- and **(c):** ZnSe-nanocluster modified rutile $TiO_2$ (110).

Reproduced from [106], 2014, The Royal Society of Chemistry.

**Figure 11** shows the atomic structure of ZnO, ZnS and ZnSe-nanocluster modified rutile (110). The computed adsorption energies are interesting in that they show that the larger ionic radius anion destabilizes the adsorption of the nanocluster at the rutile (110) surface. The Zn-X distances and Ti-X distances increase on going from O to S to Se and the longer Ti-X

distances are a potential origin of the reduced stability of the nanoclusters when adsorbed on rutile (110). This arises, because the Ti-X interaction leads to formation of the interfacial bonds between the nanocluster and the surface: longer distances between the nanocluster and the surface give weaker interactions and hence a less negative adsorption energy.

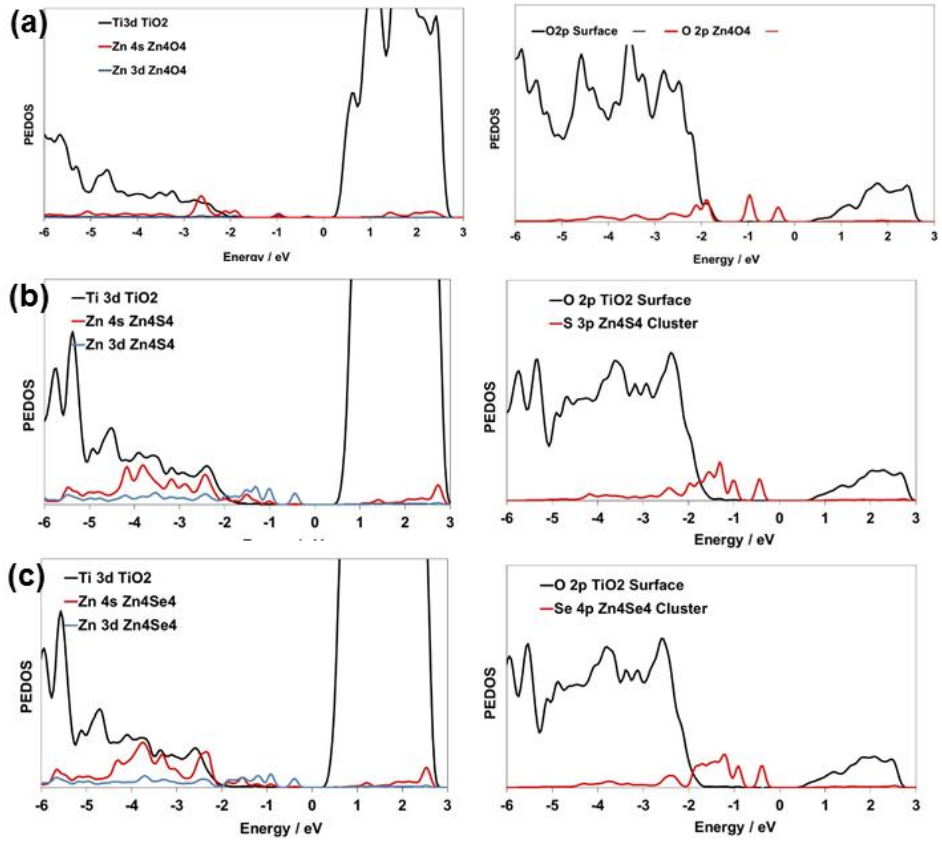


**Figure 12:** Electronic density of states projected onto Ti and Zn 3d states (left panels) and O, S and Se 2p, 3p, 4p states (right panels) for **(a):** ZnO- **(b):** ZnS- **(c):** ZnSe-modified $TiO_2$. Reproduced from [106], 2014, The Royal Society of Chemistry.

In **Figure 12** we show the PEDOS for ZnX modified $TiO_2$. In all cases, the modification with ZnX results in the appearance of new nanocluster derived electronic between the $TiO_2$ valence and conduction band edges, which will give an upwards shift of and a change in the nature of the valence band edge. The valence band edge is now derived from the ZnX nanocluster anion

*n*p states, which interact with Zn 3d states for X = S and Se. The alignment of the ZnO and rutile $TiO_2$ VB states is consistent with the qualitative picture from the bulk alignments [100]. A quantitative comparison is not possible as the alignments in ref [107] are determined using bulk ZnO and $TiO_2$ and we have considered only ZnO nanoclusters which will show electronic states relative to the $TiO_2$ valence and conduction bands that depend on the size of the nanocluster. The lowest unoccupied electronic states that make up the conduction band are always derived from unoccupied Ti 3d states. The upwards shift of the VB edge has the effect of reducing the energy separation between the highest occupied electronic state and the lowest empty electronic state.

For the modification of rutile $TiO_2$ with the $Zn_4O_4$ nanocluster, the gap between the highest occupied and lowest unoccupied energy states is reduced by ca. 1.5 eV (from a GGA+U calculated band gap value of 2.3 eV for unmodified $TiO_2$) that indicates a potentially large red shift in light absorption with ZnO modification of $TiO_2$. Reductions in the gap between the highest occupied and lowest unoccupied energy states of 1.6 eV and 1.8 eV are seen for ZnS and ZnSe, as a result of a slightly larger upshift of the occupied nanocluster states compared to ZnO. This change in the gap between the highest occupied and lowest unoccupied energy states with ZnX modified $TiO_2$ is consistent with experimental results in refs. [108-111].

For smaller $Zn_2O_2$, $Zn_2S_2$ and $Zn_2Se_2$ nanoclusters (see Ref [106]), there are some significant differences for different anions: For X = S and Se, the highest energy occupied states lie significantly above the $TiO_2$ valence band edge, whereas for ZnO these nanocluster derived states lie co-incident with the $TiO_2$ valence band edge. The identity of the anion in ZnX and the loading of the nanocluster on $TiO_2$ can therefore play a role in determining the size of any red shift relative to unmodified $TiO_2$. There interesting effect arising from the identity of the anion in the ZnX nanocluster upon modification of $TiO_2$ structures may provide another approach to shift light absorption in $TiO_2$ to the visible region.

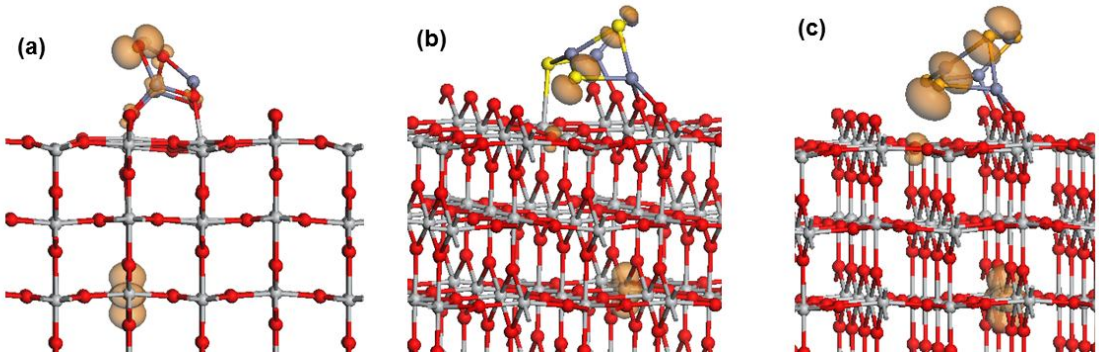


**Figure 13:** Isosurfaces of spin density for the relaxed triplet state of **(a):** ZnO, **(b):** ZnS and **(c):** ZnSe-nanocluster modified rutile $TiO_2$. Isosurfaces enclose spin density up to 0.02 eV / $Å^3$

Reproduced with permission from [106], 2014, The Royal Society of Chemistry.

Our final discussion in this section concerns the nature of the photoexcited state of ZnX-modified $TiO_2$ [106]. In the relaxed triplet state the structural relaxations trap the photoexcited electron and hole, which is shown in **Figure 13**. In all ZnX-$TiO_2$ structures, a localised reduced $Ti^{3+}$ species is found in a subsurface layer of the rutile (110) surface, forming a well-known polaron state. Computed Bader charges of this Ti in each ZnX-$TiO_2$ structure are *ca*. 1.72 electrons and the spin magnetisations are *ca*. 0.90 electrons; these are consistent with formation of a reduced $Ti^{3+}$ ion. When we examine the local geometry around this Ti site, there is a typical elongation of 0.1 - 0.18 Å in the $Ti^{3+}$-O distances compared to $Ti^{4+}$-O distances, which is consistent with formation of a polaronic $Ti^{3+}$ species.

The nature of the photoexcited hole depends on the anion. For ZnO- and ZnS-$TiO_2$, the hole is essentially localised on a two coordinated oxygen atom in each ZnX nanocluster, as shown in figure 13 (a) and (b), with a very small spreading of the hole density onto neighbouring Zn and anions; the computed Bader charge is 6.7 electrons, with a spin magnetisation of *ca*. 0.80 electrons, typical of a localised oxygen hole within the GGA+U approach. Furthermore, the geometry around the hole site shows an elongated Zn-O distance of 0.12 Å (ZnO) and 0.12 Å

(ZnS) Interestingly, for ZnSe-modified $TiO_2$, the hole spreads over two anion sites: 70 % of the hole on a two-fold coordinated Se site and 25 % of the hole on 3-fold coordinated Se site, with elongations of 0.12 Å in Zn-Se distances involving hole carrying Se sites. However, it is clear that the modification of $TiO_2$ with ZnX nanoclusters results in electron and hole separation upon photoexcitation which will decrease charge recombination.

**Table 3** shows the calculated vertical singlet-triplet energy, relaxed singlet-triplet energy and the relaxation energy for each nanocluster. The modification of rutile (110) with the ZnX nanoclusters induces a reduction in the singlet-triplet energies of rutile (110). The ZnS and ZnSe nanoclusters induce a significantly larger change in the singlet-triplet energy of $TiO_2$ compared to ZnO, with the ZnSe modification inducing the largest reduction in this energy. The results show that changing the anion in ZnX nanocluster modified $TiO_2$ allows tuning of the magnitude of the energy gap compared to unmodified $TiO_2$, at the same time displaying electron and hole separation by virtue of the nature of the nanocluster-modified surface concept.

**Table 3:** Computed vertical and relaxed singlet triplet energies, denoted as $E^{vertical}$ and $E^{S-T}$. $E^{relax}$ is the energy gained when the photoexcited state is allowed to relax.

| **Structure** | **$E^{vertical}$ / eV** | **$E^{S-T}$ / eV** | **$E^{relax}$ / eV** |
|---|---|---|---|
| $Zn_4O_4$-$TiO_2$ | 2.05 | 1.44 | 0.61 |
| $Zn_4S_4$-$TiO_2$ | 1.60 | 0.61 | 0.99 |
| $Zn_4Se_4$-$TiO_2$ | 1.30 | 0.34 | 0.96 |

## 5. Surface Modification of $TiO_2$: Synergies Between Theory and Experiment

The DFT work we have described in Section 3 gives clear insights and predictions into the effect of metal oxide nanocluster modification of $TiO_2$ and demonstrates that this strategy can induce a red shift in the absorption edge and promote electron and hole separation. Naturally, the results of these extensive simulation studies have to be compared to experimental work; a short description of selected examples of experimental work on surface modified $TiO_2$ was given in Section 2.

To confront the results of the simulation work, we have collaborated extensively with the group of Prof. Tada in Japan who have been active in synthesising and characterising surface modified $TiO_2$ materials, primarily for oxidation reactions. In progressing the deployment of these photocatalysts, successful demonstrations of water splitting or $CO_2$ activation remain to be undertaken and we hope that this Progress Report will spur on further experimental studies of these novel materials systems.

In this section, we review experimental work on metal oxide nanocluster-modified $TiO_2$ and make comparisons with our simulation results. Some results from experimental work in refs [77,78] on CuO- and $FeO_x$-modified $TiO_2$ were briefly described to highlight the experimental activities on these materials and herein we expand and discuss the correspondence between the experimental and simulation results.

In figure 3 key experimental results for CuO and $FeO_x$-modified $TiO_2$ are shown. Considering firstly CuO-modified $TiO_2$, the DFT simulations predicted a red shift in the absorption edge on both rutile and anatase[77] when modifying with CuO nanoclusters. The magnitude of the red shift depends on the coverage of the nanocluster modifier on $TiO_2$, which corresponds to the loading of the nanocluster in the experiments. The origin of the red shift is a very interesting aspect of this particular system. When we examine the valence band photoelectron spectroscopy results in figure 3(c), there appears to be a loading effect on the upwards shift of the VB edge, suggesting two distinct regimes depending on the loading of CuO. Specifically at the lowest loadings, the upshift of the valence band edge is small and then at a loading of

1.30 Cu/nm$^2$, there is a significant increase in the upwards shift. However, the red shift in the absorption edge appears not to show this same dependence on the loading. A possible explanation suggested by our simulation results is that for low CuO coverages the empty Cu 3d states characteristic of $Cu^{2+}$ lie in the valence to conduction band energy gap, with a small upshift of the valence band edge so that excitation is into empty Cu 3d states. With increasing CuO coverage, the occupied and empty CuO states move to higher energy, the empty Cu 3d states move to higher energy than the $TiO_2$ conduction band edge and there is an upshift of the valence band edge as a result of the introduction of CuO derived states. This manifests as the strong upwards shift of the valence band edge in the photoelectron spectroscopy results in figure 3. It is interesting to note that for these surface modified $TiO_2$ systems, experimental results show an upwards shift of the valence band edge of the composite system relative to unmodified $TiO_2$, compared to doping which usually results in the formation of states in the gap, not necessarily shifting the valence band edge.

For $FeO_x$ modified $TiO_2$, the simulations predict that irrespective of the oxidation state of iron, the valence band edge is shifted to higher energy as a result of new $FeO_x$ derived electronic states appearing above the $TiO_2$ valence band edge. This results in the experimentally observed red shift in the absorption edge and the upshift of the valence band edge seen in the photoelectron spectroscopy results.

Turning now to p-block metal oxide modified $TiO_2$, we firstly consider the effect of the Sn oxidation state on the properties of $SnO_2$- and SnO-modified $TiO_2$. In **Figure 14** (a) we show experimental results for the UV-vis and the valence band photoelectron spectroscopy spectrum for $SnO_2$ modified anatase [90]. The modification of anatase with $SnO_2$ results in no change in the absorption edge (data shown for one coverage), irrespective of the coverage of $SnO_2$. The VB edge shows no shift from unmodified anatase which is consistent with no shift in the absorption edge; the inclusion of $SnO_2$ and SnO data also indicates that these bulk materials are not present. Thus, $SnO_2$ has no impact on anatase. This is rationalised through

the DFT simulations which show that the $SnO_2$ electronic states lie below the anatase valence band edge and above the anatase conduction band edge.

The situation is very different when SnO-modified $TiO_2$ is considered, with experimental results shown in figure 14 (b) [103]. Here the effect of SnO is to induce a significant red shift in the absorption edge compared to unmodified $TiO_2$ (spectrum marked "inf" in figure 14 (b)); the size of the red shift can be up to 0.73 eV which is consistent with the large reduction in the energy gap predicted from our simulations in ref [86]. The same authors also modified $ZnGa_2O_4$ with SnO and $SnO_2$ [94] and found that only the modification with SnO can induce the red shift in the absorption edge while there is no effect resulting from $SnO_2$ modification. From our simulation results we can assert that the same mechanism is operating for SnO-modified $TiO_2$ and $ZnGa_2O_4$, namely that the modification with SnO introduces new Sn 5s/5p-O2p derived states that push the valence band edge to higher energy.

In the $Sn^{4+}$ oxidation state, the 5s and 5p states of Sn are empty and so cannot contribute to the valence band region. In fact the effect of $SnO_2$ can depend on the identity of the oxide being modified: in our experimental-simulation comparison of $SnO_2$ modified rutile and anatase only modification of rutile had an effect [91]. This was indicated by a small red shift in light absorption and an enhancement of visible light activity over unmodified rutile. Our DFT simulations proposed that empty Sn 5s states can be found very close to the conduction band edge of rutile thus imparting a small red shift in light absorption and electrons can be excited from the $TiO_2$ valence band into these empty Sn electronic states. The properties of $SnO_2$-modified $ZnGa_2O_4$ follow similarly – namely that there are no $SnO_2$ states that will shift the valence or conduction band edges to induce a red shift. While some $Sn^{4+}$ was present in the SnO-modified materials, there is still sufficient uoxidised SnO present to modify the properties of $TiO_2$.

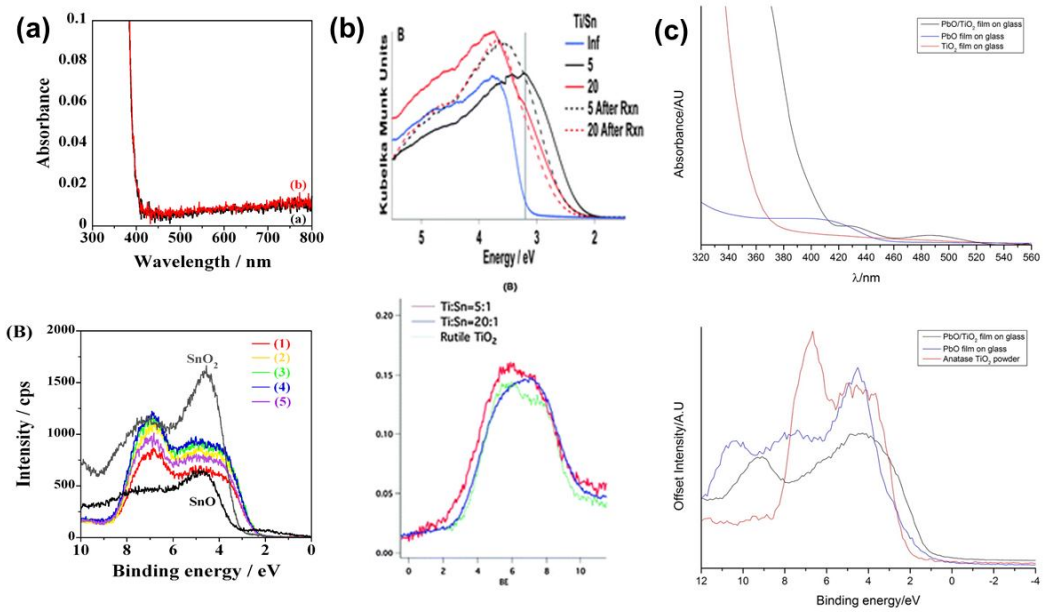


**Figure 14: (a):** Experimental UV-vis spectrum for unmodified anatase $TiO_2$ (black trace) and $SnO_2$-modified anatase $TiO_2$ (red trace) and valence band photoelectron spectrum comparing unmodified $TiO_2$ (red line), different loading of $SnO_2$-modified anatase (yellow, green, blue, purple lines), SnO and $SnO_2$. **(b):** Experimental UV-vis spectrum for unmodified $TiO_2$ (blue trace, indicated "inf") and SnO-modified $TiO_2$ (red and black traces) and valence band photoelectron spectrum comparing unmodified $TiO_2$ (green line), and different loading of SnO-modified $TiO_2$ red and blue lines). **(c):** Experimental UV-vis spectrum for unmodified $TiO_2$, PbO film and PbO-modified $TiO_2$ and valence band photoelectron spectrum comparing unmodified $TiO_2$, PbO film and PbO-modified $TiO_2$.

(a): Reproduced with permission from [90], 2012, RSC

(b): Reproduced with permission from [103], 2013, Royal Society of Chemistry

(c): Reproduced with permission from: [102], 2014, American Chemical Society

In ref [102], PbO-modified anatase $TiO_2$, was studied and the results compared to our DFT simulations that were described in Section 3. Figure14 (c) shows the UV-vis spectrum and the valence band photoelectron spectrum. In the UV-vis spectrum the modification with PbO

gives a significant red shift in the absorption edge; in addition, it is clear that the spectrum is rather different compared with unmodified $TiO_2$ and pure PbO films showing that the PbO modification does indeed change the light absorption characteristics of $TiO_2$. Further results from the valence band photoelectron spectrum show that the valence band edge of PbO-$TiO_2$ is shifted to higher energy after modification compared to the unmodified anatase film – a 1 eV shift in the valence band edge is determined. The experiments also show that no $PbO_2$ phases were present, indicating the stability of the PbO composite material.

Further experiments to examine both oxidation states of Sn or Pb oxides on the same $TiO_2$supports would provide further confirmation of our results, but the work described in refs [90,91,93,94,102,103], supports our DFT results and there is a good correspondence between the findings of DFT simulations of these p-block metal oxide nanocluster modified systems and the available experimental results. A particularly interesting insight is that the oxidation state of Sn or Pb can be used to control both the appearance of a shift in the absorption edge and the mechanism underlying this shift. The experimental work indicates that these nanocluster-modified $TiO_2$ composite materials can be prepared using standard techniques, such as CVD [102], ALD [93] and Chemisorption-Calcination [73], using non-critical materials. In addition, the materials appear to be stable over time and under illumination, which is a significant advantage over, e.g. CdS or similar semiconductor modifiers which oxidise under illumination.

## 6. Perspective

We have described in this Progress Review our DFT simulation work on a new class of photocatalyst materials, that is rutile and anatase $TiO_2$ modified with nanoclusters of metal oxides (with some preliminary work on ZnS and ZnSe) and presented some comparisons with experiment. Our results predict some interesting effects arising from this modification,

namely the potential for red shifting the absorption edge towards the visible region of the electromagnetic spectrum and the separation of photogenerated electrons and holes. The former will allow a broader range of the solar spectrum to be utilised while the latter will ensure that recombination of photogenerated electrons and holes is reduced by enhancing the charge carrier separation. This will enhance the photocatalytic activity over unmodified $TiO_2$.

In experimental work from a number of groups [73,77,78,89-94,102,103,112-117] metal oxide nanocluster modified $TiO_2$ materials have been prepared and the results from these studies are consistent with the DFT results. It is interesting to note that where no effect of the modifier is observed experimentally, the DFT simulations are able to show similar behaviour. Apart from this example of $SnO_2$-modified anatase, the composite systems fabricated to date all show red shifts towards visible light absorption and generally result in an upwards shift of the valence band edge. Importantly, there are no isolated states found between the valence band and the Fermi level that would be typical of metal species incorporated into the $TiO_2$ lattice, the so-called doping scenario, indicating that the modifiers are present in their oxide form. This difference between doping and surface modification should not result in the formation of states that trap charge carriers, thus reducing the photocurrent. For an interesting example of a doped $TiO_2$ system, we consider N-F co-doped $TiO_2$ [118] which shows visible light absorption, but no photocurrent. The surface modification approach has the potential to alleviate some of these issues with doped $TiO_2$.

There have been other experimental studies of surface modified $TiO_2$ photocatalysts in recent years. Tang et al [112] prepared NiO-modified $TiO_2$ using the CCC approach of Tada for visible light mediated functionalization of the $sp^3$ C–H bond in the cyclization reaction of *N*,*N*-dimethylaniline with maleimides to form tetrahydroquinoline products. Actually, this is also the first report of using surface modified $TiO_2$ for organic synthesis. The high thermal and photochemical stability of the composite materials also allowed them to be used for multiple cycles. Liu et al [113] prepared NiO modified $TiO_2$ through impregnation and

calcination and applied the resulting photocatalyst in $H_2$ production from glycerol and water. A reduction of 0.58 eV in the band gap allowed visible light to be used and the activity was constant over a 12 hour period. Jin et al [114] prepared $Co_2O_3$-modified $TiO_2$ using the CCC technique and found that it operates under both illumination and in dark for degradation of organic pollutants (2-naphthol and formic acid), thus imparting both thermal- and photocatalytic activity to $TiO_2$. Uddin et al [115] studied $RuO_2$-modified $TiO_2$ composite materials, that were prepared by impregnation with different $RuO_2$ loadings. Methylene orange degradation was studied with larger rate constants than P25 as the control for unmodified $TiO_2$. Photoreforming of methanol to produce $H_2$ was also studied. Li [116] studied $Cu_2O$-modified $TiO_2$ nanosheets in a one-pot hydrothermal reaction showing higher visible light activity compared to N-doped $TiO_2$. The formation of heterojunctions between the ultra-small $Cu_2O$ particles resulted in enhanced electron-hole separation over unmodified $TiO_2$. Wang et al [117] also studied $Cu_2O$-modified $TiO_2$ prepared by impregnation synthesis. A red shift in light absorption was found. Propane photo-oxidation was remarkably improved over unmodified $TiO_2$, and an interesting result is that the stability of $Cu_2O$ was enhanced over pure $Cu_2O$ during the propane oxidation process, highlighting the role played by the composite structure.

Consideration of the relative energies of the electronic states of the metal oxide modifiers allows us to examine the mechanism of visible light absorption and enhanced photocatalytic activity of metal oxide modified $TiO_2$. As an example, **Figure 15** shows a comparison of nano-scale/particle (left side) and molecular scale/nanocluster (right side) $Fe_2O_3$-modified $TiO_2$ composite structures. In the nanoparticle-$TiO_2$ system, the energy levels of the two components are little modified (with a similar scenario operating in molecular dye and quantum dot sensitised $TiO_2$), so that the energy bands are those of $Fe_2O_3$ and $TiO_2$. When a visible light photon is absorbed, there is an excitation of electron from the valence band to the conduction band of $Fe_2O_3$ (band gap of 2.2 eV). However, the resulting conduction band

energy is too low to allow the electron to transfer to conduction band of $TiO_2$ and the excited electron will recombine with a valence band hole. Although visible light absorption takes place, this composite system does not result in any visible-light photocatalytic activity [119]. For the example of quantum dot and dye sensitised $TiO_2$, the modifier conduction band lies higher in energy than the $TiO_2$ conduction band so that the excited electron transfers to $TiO_2$. The problem with these composite systems is that the quantum dot material is easily oxidised and this deactivates the quantum dot, placing limits on the use of this particular composite system in photocatalysis.

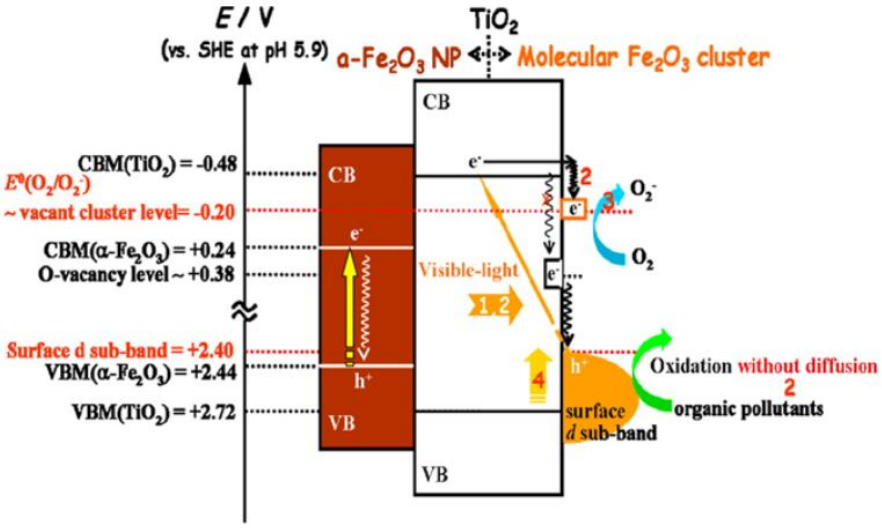


**Figure 15:** A comparison of the energy bands of nanoparticle $Fe_2O_3$-modified $TiO_2$ (a-$Fe_2O_3$ NP) and molecular sized $Fe_2O_3$ nanocluster-modified $TiO_2$ (Molecular $Fe_2O_3$ cluster) to highlight differences between nanoparticle and nanocluster modification of $TiO_2$.

Reproduced from [77], 2014, American Chemical Society

In contrast, the significant advantage offered by our approach of molecular scale nanocluster modification of $TiO_2$, is the nanoclusters show discrete energy levels whose position depends on structure and composition. The surface modification of $TiO_2$ by these molecular sized

nanoclusters generally raises the VB-maximum with no change to the CB-minimum; while there are some systems where the opposite occurs, the majority of $TiO_2$ surface modification work results in a valence band change. The origin of this is formation of the new interfacial M-O-Ti bonds formed by the strong $MO_x$-nanocluster-$TiO_2$ interaction. In addition, the nanocluster modifiers tend to have low coordinated metal and oxygen sites, do not display bulk-like structures or surface facets (in contrast nanoparticles of oxides can show surface facets that may not facilitate formation of new interfacial bonds to $TiO_2$). The low coordinated sites can form new bonds to the surface and this strong interaction results in strong electronic coupling that perturbs the electronic structure of $TiO_2$, modifying the valence or conduction bands as appropriate. This perturbation can shift the valance band edge of $TiO_2$ upwards and induce a red shift in light absorption into the visible region, which meets the primary requirement for visible light active photocatalysts.

Visible-light absorption triggers excitation of an electron from the highest energy nanocluster derived valence band states into the empty conduction band of the $TiO_2$ support and this generates the charge carriers (electrons and holes). The separation of the electrons and holes by virtue of the nanocluster modified structure and resulting band edge character described above ensures charge carrier separation and reduces recombination of electrons holes. The DFT calculations of the photoexcited state show that electrons tend to localise on the $TiO_2$ support and holes localise onto low coordinated oxygen sites in the supported nanocluster, ensuring they are well separated. Experimental indications of enhanced charge separation comes from photoluminescence results, in which the composite system is excited and emission of light resulting from charge recombination is monitored, e.g. refs [50-52,77,78,89-91]. In these studies, while unmodified $TiO_2$ shows significant PL with a characteristic PL emission at *ca*. 540 nm, the modification with oxide nanoclusters removes this characteristic PL feature. This indicates that excited electrons are not trapped in $TiO_2$, where they would recombine with holes. The reduction in recombination is then consistent with enhanced

photocatalytic activity for degradation of different molecules, mediated by holes. The surface modified $TiO_2$ composite materials thus meet the second requirement for an active photocatalyst.

Some key factors in the performance of surface modified $TiO_2$ using molecular scale MOx nanoclusters include:

A high level of control of the loading of the MOx nanoclusters on the $TiO_2$ support is a key factor for good visible-light activity [77]. The experimental studies show that the loading determines the upshift of the valence band edge of modified $TiO_2$, which tends to move to higher energy with higher loading and increases the extent of the red shift. However, if the oxidation of a target molecule occurs by hole oxidation, e.g. for 2-naphthol or phenol, is it known that there is a loading of the oxide nanoclusters beyond which the photocatalytic activity drops off, that is activity (measured by rate constant) reaches a maximum at some loading and then reduces at higher loading. The upshift of the valence band with modification lowers the oxidizing ability of the holes (because the VB edge becomes more negative, relative to the normal hydrogen electrode). At some loading the rise in the VB energy will be too high so as to prevent hole oxidation. There is thus an optimum loading of the metal oxide nanocluster modifier which will depend on the identity of the oxide nanocluster and the target molecules. From the DFT simulations the corresponding factor is the size (composition) of the supported nanocluster which we have shown determines the shift of the valence band edge relative to unmodified $TiO_2$.

Interestingly, the effect of surface modification on the photocatalytic activity of $TiO_2$ can also depend on the crystal form of $TiO_2$, which is exemplified by the modification of rutile and anatase $TiO_2$ with $SnO_2$. Modification of rutile leads to an increase in UV activity, but for modified anatase, there is no effect. On the other hand, for other metal oxides, such as NiO or PbO, the crystal form of $TiO_2$ has little effect. The exact importance of this effect requires further work.

The nature of the cation in the nanocluster modifier can be important to tune the properties of the composite system. This is particularly interesting where a metal has two oxidation states which impart very different properties to their parent oxide, such as $Sn^{2+/4+}$ or $Pb^{2+/4+}$, where the change in Sn oxidation state from 2+ to 4+, by removing the stereochemical lone pair in Sn that modifies the $TiO_2$ valence band, change entirely the effect of $SnO_x$ modification of $TiO_2$. For $PbO_x$, the change in oxidation state changes the mechanism of band gap reduction. Other oxides where this oxidation state effect could be exploited include $Cu_2O$/CuO, $CoO_x$ or $MoO_x$ and this is an interesting avenue for further work.

The molecular sized nanoclusters show useful features that can be exploited in these composites. The most important features are the non-bulk like structure and the presence of low coordinated metal and oxygen sites. As described in our previous work [81] $TiO_2$ nanoclusters show 4-fold coordinated Ti and singly coordinated titanyl O species that are stable sites for localisation of electrons and holes. $TiO_2$ nanoclusters supported on rutile have titanyl oxygens on which holes localise and electrons localise onto the surface. With a wide band gap substrate, such as $TiO_2$-modified $La_2O_3$ [81], the electron localises onto a 4-coordinate Ti species in the nanocluster and the position of the conduction band edge is shifted to lower energy. The presence of these non-bulk sites in the nanocluster is important for localising photogenerated electrons and holes.

**7. Summary**

This Progress Report has shown that a combination of DFT-level simulations and detailed experiments is a powerful approach to develop a new class of $TiO_2$-based photocatalysts, for which the origins of enhanced visible light activity, at least for oxidation reactions, are well understood and the activity of these new materials is very promising. Simulations are able to both predict and understand experimental results guiding the design of these new photocatalysts in a rational and efficient manner. In moving forward there are a number of

interesting avenues that need to be explored to further develop these new materials. These include: **(1)** preparation of nanocluster modified $TiO_2$ with industrially relevant techniques such as CVD or atomic layer deposition and understanding how the deposition/growth parameters impact on the structure and photocatalytic properties of modified $TiO_2$, **(2)** characterisation of the structural modifications – it is necessary that the ability to examine the atomic level structures of these composites be enhanced to determine what is the precise nature of the composite and the $TiO_2$ modifier interface, **(3)** exploiting this concept to develop photocatalysts that are active for reduction reactions – the band energies of $TiO_2$ are such that it is active for hole oxidation, as a result of the favourable valence band energy, but the conduction band energy is not particularly favourable for, e.g. $CO_2$ reduction. Modifications of $TiO_2$ will only shift the conduction band to lower energies which makes reduction even more difficult to perform. Thus, new materials will be required in which a suitable conduction band edge is present and the surface modification may then be used to red shift the absorption edge and provide sites for electron localisation and subsequent transfer to $CO_2$, thus activating this difficult to activate molecule, **(4)** moving beyond environmental applications to oxidising water for hydrogen production – a stable, non-toxic, visible light activated photocatalyts made of eath abundant, non-critical materials will be required to drive this technology forwards.

To conclude, we have presented a review of progress to date in the exciting area of surface modified $TiO_2$ photocatalysts that is driven by simulation, working in collaboration with experiment. This work has delivered new materials that are visible light active and show enhanced photocatalytic activity for oxidation reactions compared to unmodified $TiO_2$. The DFT simulations have provided key insights into the effect of nanocluster modifications of $TiO_2$, e.g. the structure, band gap modification and charge carrier localization, while giving clear guidelines to enhance the photocatalytic activity of $TiO_2$, but should be applicable to other photocatalysts. Spectroscopic experiments and our DFT simulation have revealed that the key effect of surface modification is to shift the VB-maximum of $TiO_2$ to higher energy

due to the formation of multiple new metal-O-Ti interfacial bonds, promoting both visible-light absorption and enhancing charge carrier separation. This new coupling of molecular scale metal oxide nanoclusters and $TiO_2$ shows great promise as a photocatalyst that can use solar energy.

Acknowledgements

We acknowledge support from Science Foundation Ireland (SFI) through the Starting Investigator Research Grant Program, project ``EMOIN'', grant number SFI 09/SIRG/I1620, SFI through the US-Ireland R&D Partnership Program, grant number SFI 14/US/E2915 and the European Commission through the COST Action CM1104 ``Reducible Metal Oxides, Structure and Function''. We acknowledge access to computing resources at Tyndall provided by SFI and by the SFI and Higher Education Authority funded Irish Centre for High End Computing and the European Commission Partnership in Advanced Computing (PRACE, contracts RI-261557, RI-283493 and RI-312763) for access to the UYBHM Computer at Istanbul Teknik Universitesi and the JUROPA Computer at Forschungszentrum Juelich through the DECI initiative. We are honoured to acknowledge our collaboration with Prof. H. Tada on surface modified $TiO_2$ and for his valuable insights and discussions into these novel photocatalyst materials and our collaboration with Prof. J. A. Byrne (Ulster) and Profs. K. A. Gray, J. Notestein and E. Weitz (Northwestern) on photocatalytic $CO_2$ reduction.

Received: ((will be filled in by the editorial staff))
Revised: ((will be filled in by the editorial staff))
Published online: ((will be filled in by the editorial staff))

**References**

[1] S. Roy, O. K. Varghese, M. Paulose, C. A. Grimes, *ACS Nano*, 2010, *4*, 1259,

[2] N. S. Lewis, D. G. Nocera, *Proc. Nat. Acad. Sci.*, 2006, *103*, 15729

[3] *International Energy Outlook 2013;* US Energy Information Administration, US DoE, Washington DC, 2013

[4] P. D. Tran, L. H. Wong, J. Barber, J. S. C. Loo, *Energy and Environmental Science*, 2012, *5*, 5902

[5] Intergovernmental Panel on Climate Change Emissions Scenarios, Cambridge University Press, 2000

[6] UN world energy assessment report: energy and challenges of sustainability 2003

[7] International Energy Agency Outlook 2008

[8] IPCC Data: http://www.ipcc-data.org/observ/ddc_co2.html (accessed October 2015)

[9] US DoE Office and Science Grand Challenges http://science.energy.gov/bes/efrc/research/grand-challenges/ (accessed October 2015)

[10] The European Commission Climate and Energy Package: COM (2008) 30

[11] Renewable Heating and Cooling Technology platform, http://www.rhc-platform.org (accessed October 2015), and PV Technology Platform, www.eupvplatform.org (accessed October 2015)

[12] Department of Energy, Communications and Natural Resources, Energy White paper 2007: Delivering a Sustainable Energy Future for Ireland.

[13] The National Renewable Energy Plan: http://www.dcenr.gov.ie/Energy/Sustainable+and+Renewable+Energy+Division/ (accessed October 2015)

[14] G. A. Olah, *Angew. Chem. Intl. Ed.*, 2005, *44*, 2636

[15] K. H. Nealson, P. G. Conrad, *Phil Trans Royal Soc B*, 1999, *354*, 1923

[16] *World Energy Scenarios: Composing energy futures to 2050*. World Energy Council, 2013

[17] S. G. Kumar, L. G. Devi, *J. Phys. Chem. A*, 2011, *115*, 13211

[18] K. Hashimoto, H. Irie, A. Fujishima, *Jap. Journal Appl. Phys.*, 2005, *44*, 8269

[19] M. Pelaez, N. T. Nolan, J. A. Byrne, S. C. Pillai, M. K. Seery, P. Falaras, A. G. Kontos, P. S. M. Dunlop, J. W. J. Hamilton, J. A. Byrne, K. O'Shea, M. H. Entezari, D. D. Dionysiou, *Appl. Cat. B.*, 2012, *125*, 331

[20] S. C. Pillai, U. L. Stanger, J. A. Byrne, A. Perez-Larios, D. D. Dionysiou, *Chem. Eng. J.*, 2015, *261*, 1

[21] V. Etacheri, C. Di Valentin, J. Schneider, D. Bahnemann, S. C. Pillai, *J. Photochem and Photobiol C: Photochemistry Reviews*, 2015, *25*, 1

[22] M. Ni, K. M. Leung, D. Y. Leung, K. Sumathy *Renewable and Sustainable Energy Reviews*, 2007, *11*, 401

[23] A. L. Linsebigler, G. Lu, J. T. Yates Jr, *Chemical Reviews*, 1995, *95*, 735

[24] A. Wold, *Chemistry of Materials*, 1993, *5*, 280

[25] N. Serpone, *J. Phys. Chem. B*, 2006, *110*, 24287

[26] A. Fujishima, X. Zhang, D. A. Tryk, *Surface Science Reports*, 2008, *63*, 515

[27] A. Fujishima, T. N. Rao, D. A. Tryk, *Journal of Photochemistry and Photobiology C: Photochemistry Reviews*, 2000, *1*, 1

[28] J. T. Yates, *Surface Science* 2009, *603*, 1605

[29] R. Asahi, T. Morikawa, K. Ohwaki, K. Aoki, Y. Taga, *Science*, 2001, *293*, 269

[30] M. Kapilashrami, Y. Zhang, Y-S. Liu, A. Hagfeldt, J. Guo, *Chem. Rev.*, 2014, *114*, 9662

[31] X. L. Nie, S. P. Zhou, G. Maeng and K. Sohlberg, *Int. J. Photoenergy*, 2009, 294042

[32] Y. Gai, J. Li, S-S Li, J-B. Xai, S-H. Wei, *Phys. Rev. Lett.*, 2009, *102*, 036402

[33] H. Zhang, G. Chen, D. W. Bahnemann, *J. Mater. Chem.* 2009, *19*, 5089.

[34] G. Liu, L. Wang, H. G. Yang, H. M. Cheng and G. Q. Lu, *J. Mater. Chem.* 2010, *20*, 831

[35] G. Wang, Y. Ling, Y. Li, *Nanoscale*, 2012, *4*, 6682

[36] X. Pan, M-Q. Yang, X. Fu, N. Zhang Y-J. Xu., *Nanoscale*, 2013, *5*, 3601

[37] L-B Xiong, J-L. Li, B. Yang, Y. Yu, *J. of Nanomaterials*, 2012, Art. 831524 (doi:10.1155/2012/831524)

[38] H. Liu, H. T. Ma, X. Z. Li, W. Z. Li, M. Wu, X. H. Bao, *Chemosphere*, 2003, *50*, 39

[39] X. Chen, L. Liu, P. Y. Yu, S. S. Mao, *Science*, 2011, *331*, 746

[40] A. Sirisuk, E. Klansorn, P. Praserthdam, *Catalysis Communications*, 2008, *9*, 1810

[41] J. Jun, M. Dhayal, J. H. Shin, J. C. Kim, N. Getoff, *Radiation Physics and Chemistry*, 2006, *75*, 583

[42] D. R. Park, J. Zhang, K. Ikeue, H. Yamashita, M. Anpo, *J. Catal.*, 199, *185*, 114

[43] K. Suriye, P. Praserthdam, B. Jongsomijt, *Appl. Surf. Sci.*, 2007, *253*, 3849

[44] J. Nowotny, T. Bak, M. K. Nowotny, L. R. Sheppard, *Int. J. Hydrogen Energy*, 2007, *32*, 2630

[45] M. K. Nowotny, L. R. Sheppard, T. Bak, J. Nowotny, *J. Phys. Chem. C*, 2008, *112*, 5275

[46] T. Thompson, J. T. Yates Jr., *Top. Catal.*, 2005, *35*, 197

[47] G. Liu, F .Li, D.-W. Meng, D.-M. Tang, C. Liu, X. Ma, G. Q. Lu and H.-M. Cheng, *Nanotoechnology*, 2008, *19*, 025606

[48] C. L. Muhlich, Y. Zhou, A. M. Holder, A. W. Weimer, C. B. Musgrave, *J. Phys. Chem. C*, 2012, *116*, 10138

[49] G. M. Wang, H. Y. Wang, Y. C. Ling, Y. C. Tang, X. Y. Yang, R. C. Fitzmorris, C. C. Wang, Z. J. Zhang, Y. Li, *Nano Lett.*, 2011, *11*, 3026

[50] H. Y. Wang, G. M. Wang, Y. C. Ling, M. Lepert, C. C. Wang, Z. J. Zhang, Y. Li, *Nanoscale*, 2012, *4*, 1436

[51] Y. Tamaki, A. Furube, M. Murai, K. Hara, R. Katoh, M. Tachiya, *Phys. Chem. Chem. Phys.*, 2007, *9*, 1453

[52] A. O. T. Patrocinio, J. Schneider, M. D. France, L. M. Santos, B. P. Caixeta, A. E. H. Machado, D. W. Bahnemann, *RSC Adv.* 2015, *5*, 70536

[53] A. Green, E. Palomares, S. A. Haque, J. R. Durrant, *Proc. SPIE (Interfacial Electron Transfer)*, 2004, *5513*, 56

[54] A. M. Peiró, C. Colombo, G. Doyle, J. Nelson, A. Mills, J. R. Durrant *Journal of Physical Chemistry B* 2006, *110* , 23255

[55] X. Wang, A. Kafizas, X. Li, S. J. A. Moniz, P. J. T. Reardon, J. Tang, I. P. Parkin and J. R. Durrant, *J. Phys. Chem. C*, 2015, *119*, 10439

[56] J. Liqiang, Q. Yichun, W. Baiqi, L. Shudan, J. Baojiang, Y. Libin, F. Wei, F. Honggang, S. Jiazhong, *Solar Energy Materials and Solar Cells*, 2006, *90*, 1773

[57] J. G. Yu, H. G. Yu, B. Chen, X. J. Zhao, J. C. Wu, W. K. Ho, *J. Phys. Chem. B*, 2003, *107*, 13871

[58] L. Q. Jing, X. J. Sun, W. M. Cai, X. Q. Li, H. G. Fu, H. G. Nou, N. Y. Fan, *Acta. Chim. Sin*, 2003, *61*, 1451

[59] V. I. Anisimov, J. Zaanen, O. K. Andersen, *Phys. Rev B*, 1991, *44*, 943

[60] S. L. Dudarev, G. A. Botton, S. Y. Savrasov, C. J. Humphreys, A. P. Sutton, *Phys. Rev. B*, 1998, *57*, 1505

[61] H. Yan, X. Wang, M. Yao, X. Yao, *Progress in Natural Science: Materials International*, 2013, *23*, 402

[62] A. D. Becke, *J. Chem. Phys.*, 1993, *98*, 5648

[63] B. J. Janesko, T. M. Henderson, G. A. Scuseria, *Phys. Chem. Chem. Phys.*, 2009, *111*, 443

[64] P. Ágoston, K. Albe, R. M. Nieminen, M. J. Puska, *Phys. Rev. Lett.*, 2009, *103*, 245501

[65] P. Rinke, A. Janotti, M. Scheffler, C. G. van de Walle, *Phys. Rev. Lett.*, 2009, *103*, 026402

[66] A. Janotti, C. G. van de Walle, in Advanced Calculations for Defects in Materials: Electronic Structure Methods, edited by A. Alkauskas, P. Deak, J. Neugebauer, A. Pasquarello, C. G. Van de Walle, Wiley, 2011

[67] A. Iwaszuk, M. Nolan, *J. Phys.: Condensed Matter*, 2011, *33*, 334207

[68] A. Iwaszuk, M. Nolan, *J. Phys. Chem. C*, 2011, *115*, 12995

[69] M. Nolan, G. W. Watson, *Surf. Sci.*, 2005, *586*, 25

[70] M. Nolan, G. W. Watson, *J. Chem. Phys.*, 2006, *125*, 144701

[71] H. Gudmundsdottir, E. O. Jonsson, H. Jonsson, *New Journal of Physics*, 2015, *17*, 083006

[72] M. Nolan, S. C. Parker, G. W. Watson, *Surf. Sci.*, 2005, *595*, 223

[73] H. Tada, Q. Jin, A. Iwaszuk, M. Nolan, *J. Phys. Chem. C*, 2014, *118*, 12077

[74] H. Irie, S. Miura, K. Kamiya, K. Hashimoto, *Chem Phys Lett*, 2008, *457*, 202

[75] H. Irie, T. Shibanuma, K. Kamiya, S. Miura, T. Yokoyama, K. Hashimoto, *App Cat B*, 2010, *96*, 142

[76] H. Tada, Encyclopedia of Surface and Colloid Science; Hubbard, A. T., Ed.; Marcel Dekker: New York, 2002

[77] H. Tada, Q. Jin, H. Nishijima, H. Yamamoto, M. Fujishima, S-i Okuoka, T. Hattori, Y. Sumida, H. Kobayashi, *Angewandte Chemie International Edition*, 2011, *50*, 3501

[78] Q. Jin, M. Fujishima, A. Iwaszuk, M. Nolan and H. Tada, *J. Phys. Chem. C*, 2013, *117*, 23848

[79] A. Iwaszuk, P. A. Mulheran, M. Nolan, *J. Mat. Chem. A*, 2013, *1*, 2515

[80] A. Iwaszuk, M. Nolan, *Phys. Chem. Chem. Phys.*, 2011, *13*, 4963

[81] M. Nolan, A. Iwaszuk, K. A. Gray, *J. Phys. Chem. C*, 2014, *118*, 27890

[82] C. Di Valentin, A. Selloni, *J. Phys. Chem. Lett.*, 2011, *2*, 2223

[83] A. Jedidi, A. Markovits, C. Minot, M. Bouzriba, M. Abderraba, *Langmuir*, 2010, *26*, 16232

[84] K. P. McKenna, M. J. Wolf, A. L. Shluger, S. Lany and A. Zunger, *Phys. Rev. Lett.*, 2012, *108*, 116403

[85] M. Nolan, *ACS Applied Materials and Interfaces*, 2012, *4*, 5683

[86] A. Iwaszuk, M. Nolan, *J. Mat. Chem. A*, 2013, *1*, 6670

[87] A. Iwaszuk, M. Nolan, *Catal. Sci. Tech.*, 2013, *3*, 2000

[88] E. Berardo, H-S. Hu, S. A. Shevlin, S. M. Woodley, K. Kowalski, M. A. Zwijnenburg, *J. Chem. Theory Comput.*, 2014, *10*, 1189

[89] A. Iwaszuk, M. Nolan, Q. Jin, M. Fujishima, H. Tada, *J. Phys. Chem. C*, 2013, *117*, 2709

[90] M. Fujishima, Q. Jin, H. Yamamoto, H. Tada, M. Nolan, *Phys. Chem. Chem. Phys.*, 2012, *14*, 705

[91] Q. Jin, M. Fujishima, M. Nolan, A. Iwaszuk, H. Tada, *J. Phys. Chem. C*, 2012, *116*, 12621

[92] M. Nolan, *Phys. Chem. Chem. Phys.*, 2011, *13*, 18194

[93] J. A. Libera, J. W. Elam, N. F. Sather, T. Rajh, N. Dimitrijevic, *Chem. Mat.*, 2010, *22*, 409

[94] V. B. R. Boppana, R. F. Lobo, *ACS Catal*, 2011, *1*, 923

[95] Y. Xia, K. Zhu, T. C. Kaspar, Y. Du, B. Birmingham, K. T. Park, Z. Zhang *J. Phys. Chem. Lett.*, 2013, *4*, 2958

[96] S. Liu, J. Yu, M. Jaroniec *Chemistry of Materials* 2011, *23*, 4085

[97] L. Wang, L. Zang, J. Zhao, C. Wang *Chem. Commun.*, 2012, *48*, 11736

[98] F. Amano, O. Prieto-Mahaney, Y. Terada, T. Yasumoto, T. Shibayama, B. Ohtani, *Chem. Mater.* 2009, *21*, 2601

[99] F. De Angelis, C. Di Valentin, S. Fantacci, A. Vittadini, A. Selloni, *Chem. Rev.*, 2014, *114*, 9708

[100] N. Sutradhar, A. K. Biswas, S. K. Pahari, B. Ganguly, A. B. Panda, *Chem. Commun.*, 2014, *50*, 11529

[101] H. G. Yang, C. H. Sun, S. Z. Qiao, J. Zou, G. Liu, S. C. Smith, H. M. Cheng, G. Q. Lu, *Nature*, 2008, *453*, 638

[102] D. S. Bhachu, S.Sathasivam, C. J. Carmalt, I. P. Parkin, *Langmuir*, 2014, *30*, 624

[103] V. B. R. Boppana, F. Jiao, D. Newby, J. Laverock, K. E. Smith, J. C. Dumas, G. Hutchings, R. F. Lobo, *Phys. Chem. Chem. Phys.*, 2013, *15*, 6185

[104] D. J. Payne, R. G. Egdell, A. Walsh, G. W. Watson, J. Guo, P-A. Glans, T. Learmonth and K. E. Smith, *Phys. Rev. Lett.*, 2006, *96*, 257403

[105] A. Walsh, D. J. Payne, R. G. Egdell, G. W. Watson, *Chem. Soc. Rev.*, 2011, *40*, 4455

[106] A. Iwaszuk, A. K. Lucid, K. M. Razeeb, M. Nolan, *J. Mat. Chem. A*, 2014, *2*, 18796

[107] J. Wang, X-L. Liu, A-Li. Yang, G-L. Zheng, S-Y. Yang, H-Y. Wei, Q-S. Zhu, Z-G. Wang, *Appl. Phys. A*, 2011, *103*, 1099

[108] V. Stengel, S. Bakardjieva, N. Murafa, V. Houskova, K. Lang, *Microporous and Mesoporous Materials*, 2008, *110*, 370

[109] S. H. Hwang, J. Song, Y. Jung, O. Y. Kweon, H. Song, J. Jang, *Chem. Comm.*, 2011, *47*, 9164

[110] C. Cheng, A. Amini, C. Zhu, Z. Xu, H. Song, N. Wang, *Sci. Rep*., 2014, *4*, 4181

[111] D. Li, Y. Zhang, W. Wu, C. Pan, *RSC Adv.*, 2014, *4*, 18186

[112] J. Tang, G. Grampp, Y. Liu, B-X Wang, F-F Tao, L-J Wang, X-Z Liang, H-Q Xiao, Y-M Shen, *J. Org. Chem.*, 2015, *80*, 2724

[113] R. Liu, H. Yoshida, S-i Fujita, M. Arai, *Appl Cat B* 2014, *144*, 41

[114] Q. Jin, H. Yamamoto, K. Yamamoto, M. Fuishima, H. Tada, *Phys. Chem. Chem. Phys.*, 2013, *15*, 20313

[115] Md. T. Uddin, O. Babot, L. Thomas, C. Olivier, M. Redaelli, M. D'Arienzo, F. Morazzoni, W. Jaegerman, N. Rockstroh, H. Junge, T. Toupance, *J. Phys. Chem. C*, 2015, *119*, 7006

[116] L. Liu, X. Gu, C. Sun, H. Li, Y. Deng, F. Gao, L. Dong, *Nanoscale* 2012, *4*, 6351

[117] D. Wang, X. Pan, G. Wang, Z. Yi, *RSC Advances* 2015, *5*, 22038

[118] J. W. J. Hamilton, J. A. Byrne, P. S. M. Dunlop, D. D. Dionysiou, M. Pelaez, K. O'Shea, D. Synnott, S. C. Pillai, *J. Phys. Chem. C*, 2014, *118*, 12206

[119] X. Lin, D-Z. Li, Q-P. Wu, X-Z. Fu, X-X. Wang, *Chem. J. Chin. Univ*. 2005, *26*, 727

The table of contents entry:
**Designer $TiO_2$ photocatalysts.** Modification of the paradigm photocatalyst $TiO_2$ with molecular sized metal oxide nanoclusters can impart visible light activity and enhanced oxidation activity. Design of the photocatalysts through Density Functional Theory simulations, together with experiment, allows rational discovery of new visible light active photocatalyst materials.

Keyword: Photocatalysis

*Michael Nolan*, Anna Iwaszuk, Aoife K. Lucid, John J. Carey and Marco Fronzi*

**Design of novel visible light active photocatalyst materials: Surface modified $TiO_2$**

ToC figure:

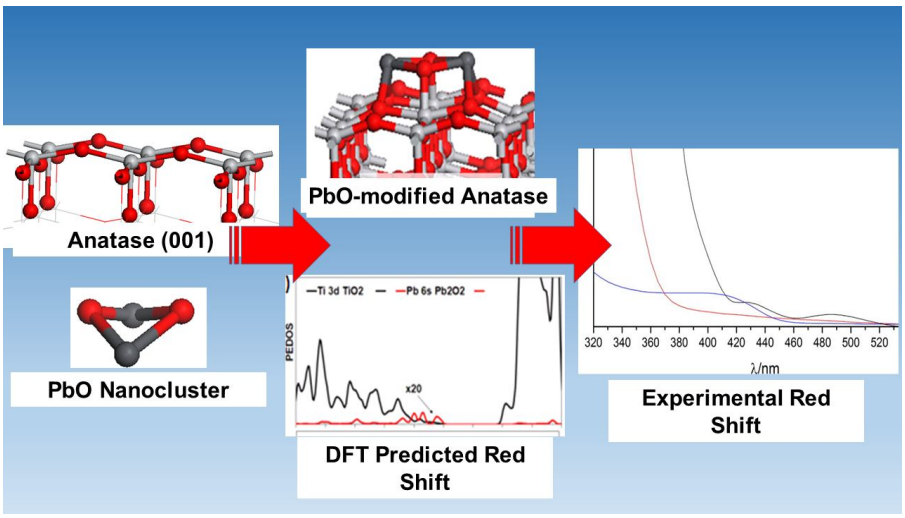

**Author Biographies:**

**Dr. Michael Nolan** is a Senior Staff Researcher at Tyndall National Institute, University College Cork. He obtained his BSc. in Chemistry and German from Dublin City University (1997), before undertaking an MEngSc and PhD in Electronic Engineering from University College Cork (1999 and 2004). He was a postdoctoral research fellow with Prof. Graeme Watson in Trinity College Dublin, using DFT to model reactivity of cerium dioxide, before joining Tyndall in 2005. Dr. Nolan leads a team of researchers focussed on modelling for the design of new photocatalysts, metal oxide surfaces and catalysis, intermetallic alloys, amorphous silicon and solvent-solute interactions.

**Dr. Anna Iwaszuk**

Dr. Anna Iwaszuk. was born in Poland. She obtained a BSc in Analytical Chemistry from Hogeschool Zeeland in the Netherlands and MSc in Chemical and Process Engineering from Technical University of Szczecin, Poland. She completed her PhD studies on surface modified $TiO_2$ photocatalysts with Dr. Michael Nolan at the Tyndall National Institute in 2014 and now works with Pfizer Pharmaceuticals, leading a team in developing active pharmaceutical ingredients.

**Ms. Aoife K. Lucid**

Aoife Lucid is a Ph.D. student in the Computational Chemistry Group in Trinity College Dublin, Ireland. She received her B.Sc in Chemical Physics from University College Cork, Ireland, in 2013. As an undergraduate she undertook research projects in the Materials Modelling for Devices Group and the Photonics Theory Group at Tyndall National Institute, Ireland. She was also awarded a FASTNET bursary for summer research in the

Electrochemical Materials and Energy Group at Tyndall National Institute. Her current research focuses on theory and simulation of interfaces in solid electrolytes for application in solid oxide fuel cells

**Dr. John J. Carey**

**Dr. Marco Fronzi**

Marco Fronzi is a researcher in the Theory, Modelling & Design centre at Tyndall National Institute, University College Cork (Ireland). After receiving his Laurea in Physics, he completed his PhD in Computational Materials Science at the University of Tor Vergata, Italy. During the course of his career he has held research positions with a range of institutions across the world, including University of Sydney in Australia, Osaka University and National Institute for Material Science in Japan, where he was awarded with the JSPS Fellowship. His research focuses on the application of theoretical-computational methodologies to understand and predict properties of surfaces, interfaces and bulk of materials of technological interest.